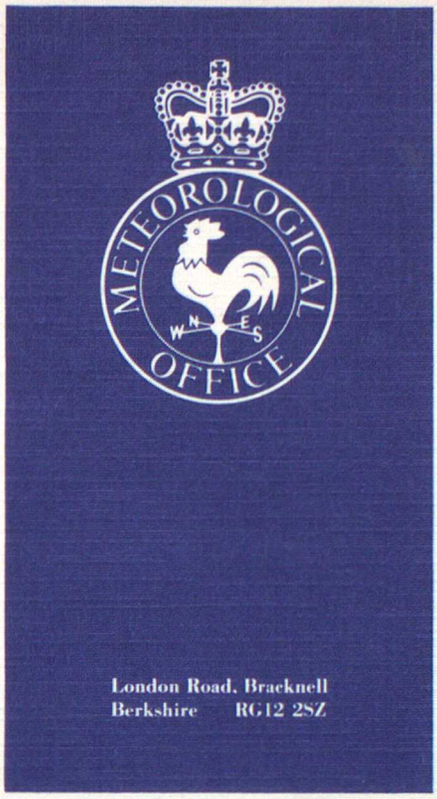

LONDON, METEOROLOGICAL OFFICE.

Met.O.15 Internal Report No.65.

Lyman-alpha total water content hydrometer: construction and testing of a prototype. By LEIGHTON,J.R., NICHOLLS,S., COOPER,G. and BARKER,R.A.L.

London,Met.Off.,Met.O.15 Intern.Rep.No.65, 1986,30cm.Pp.28,25 pls.6 Refs.

An unofficial document - not to be quoted in print.

METEOROLOGICAL OFFICE
London Road, Bracknell, Berks.

MET.O.15 INTERNAL REPORT

Number 65

Lyman-alpha Total Water Content Hygrometer:
Construction and Testing of a Prototype.

by

Leighton, J.R., Nicholls, S., Cooper, G.and Barker, R.A.L.

3rd February 1986

Cloud Physics Branch (Met.O.15)

LYMAN-ALPHA TOTAL WATER CONTENT HYGROMETER:

CONSTRUCTION AND TESTING OF A PROTOTYPE

1. INTRODUCTION

This report describes further experiments and trials on a prototype Lyman-alpha total water hygrometer eventually intended for aircraft mounting to measure fluctuations of total water content (ie. vapour + liquid/ice).

Air entering an inlet nozzle at 100 m s^{-1} (a typical aircraft speed) is decelerated and heated so that any water/ice is rapidly evaporated. The air/vapour mixture passes through a Lyman-alpha source/detector and exits through an exhaust port. The detector signal is processed to give an indication of the amount of water vapour in the sampled air.

Previous work described in Met O 15 Internal Report No. 56, showed that the evaporator configuration successfully removed all liquid water, with a time constant of ~ 0.25 s for a 1 mm drop, and that further development was justified.

Following the successful completion of this initial feasibility study a number of improvements were made to enable full wind-tunnel trials to be carried out. This paper describes these results.

2. IMPROVEMENTS TO THE ORIGINAL DESIGN

2.1) To facilitate wind tunnel testing, a suitable casing was designed and built in light alloy in order to provide a streamlined, protective cover for the evaporator, hygrometer and electronics. The exterior shape of the casing was designed to allow isokinetic sampling at the inlet port which is desirable to eliminate any possible sampling bias. To enable the final shape to be determined by wind tunnel testing an adjustable exhaust port was incorporated into the design.

Figs.1 and 2 show the probe in its latest form (Dec.'85), ie. including all modifications as discussed later in this report. Air passes into the 1 cm diameter inlet nozzle at a rate of approximately 7.8 l s^{-1} and passes through two barium titanate self thermostatting heaters which maintain their temperature at ~120 ^{o}C regardless of the air temperature or flow velocity. The heated air then passes through a static rotor and a series of three stainless steel meshes with progressively smaller holes (66 um, 48 um, 36 um) which ensures complete evaporation of any water or ice (ref. Met.0.15 Internal Report 56). The humidity mixing ratio of the heated air and water vapour is sampled and measured with a Lyman-alpha absorption hygrometer and is exhausted through an adjustable port at the rear. The probe body is supported by steel members connected to an adaptor plate (not shown) and the whole structure is constructed with watertight, flush joints to allow operation in an icing wind tunnel.

2.2) An improved Lyman-alpha hygrometer was constructed using a conventional nitric oxide photoionization chamber (Fig.3) and a

low hydrogen pressure discharge lamp as a UV source (Fig.4). Integral with the source tube is a UH_3 pellet and heater to serve as a hydrogen source. As described by Buck, these tubes are considered to be far superior to a conventional tube. A spectrally cleaner emission can be obtained using a low hydrogen pressure, DC-excited, discharge lamp. To ensure the low pressure lamp has a reasonable lifetime, any hydrogen lost to the walls of the envelope must be replaced. UH_3 , on heating, will release hydrogen until an equilibrium pressure is reached. This pressure is dependent on the temperature of the UH_3. Thus the hydrogen pressure can be maintained, whilst the tube is in use, by controlling the temperature of the UH_3. On cooling, the UH_3 re-adsorbs the hydrogen. Temperature control of the UH_3 to a preset value of ~ 130 ^{o}C is attained using a servo-controlled power amplifier to an accuracy of 0.1 ^{o}C. Experiments showed this to be equivalent to an UV detector output change of ~ 0.7% (< 0.01 g m^{-3} equivalent).

The source tube is used with a constant 210 V.d.c. at 0.5 mA , the current being set manually. The detector has a constant 70 V ion-collecting potential across its terminals. Due to the extremely small current generated by the detector (~10^{-9} A) all signal cables and circuit board tracks are carefully screened and guarded to keep all electrical noise to a minimum. The whole of the detector is housed in a brass assembly, except the window end, to assist in this noise reduction.

Since the air gap between the source and the detector dictates the length of the absorber and therefore the sensitivity of the device, it must be accurately measured and remain fixed. The gap

may be adjusted within the limits 0 mm to 10 mm. A wider gap increases sensitivity but decreases range. It was found that a good figure for this gap in terms of sensitivity and range was 5 mm which was kept constant throughout all the trials and calibrations. Adjustment of this air gap is achieved by screwing both the source and detector tubes into or out of the flow tube then locking in position by locking rings. The screw threads and locking rings also serve as airtight seals to prevent the sampled air being contaminated, and to prevent the chamber occupied by the electronics being subjected to sample air. Accurate measurement of the air gap is possible using accurately machined datum points on the tube holders.

2.3) A number of parameters were required to be monitored and recorded. These included:-

Environmental temperature

Sample temperature (at hygrometer)

Evaporator voltages and currents

Lyman-alpha source tube current

Hygrometer output voltage.

Fig. 5 shows a schematic of the electronics.

Temperatures were measured using thermistors, coupled to amplifiers and were calibrated to give repeatable temperatures to within +/- 0.1 ^{o}C.

The evaporator heater voltages (0-115 V.a.c.) and currents (0-10 A peak) were monitored using transformers and rectifiers to

bring the signal down to a level suitable for A/D sampling (0-10 V) and calibrated against a digital voltmeter to within 1 V and 0.1 A of the heater voltage and current.

The Lyman-alpha source tube current was initially adjustable and monitored via a LED display to ensure a constant emission from the tube. Later, circuitry was installed which enabled a preset constant source tube current to be maintained.

Finally, the hygrometer detector current is monitored and recorded. Since the detector current is of the order of 10^{-9} A, a high gain, first stage amplifier is used and produces an output of 0-1 V. Due to the high gain required the signal cable to this amplifier is screened and kept as short as possible. The output is amplified, in a buffer, by a factor of 4, then fed to a logarithmic amplifier which linearises the final output to a level suitable for A/D conversion (0-10 V).

2.4) Initially, data monitoring and recording used the A/D converter of a BBC model B microcomputer. This was found acceptable for the initial study but would not be able to cope with any extra channels (>4) with a suitable accuracy or sampling speed. So, using the same microcomputer, a data acquisition unit was built around an 8-channel, 12-bit A/D converter. It is desirable to record the Lyman-alpha detector output at a rate of 100 Hz and sufficient to sample the 7 other channels sequentially, interleaved with the Lyman-alpha channel. Therefore a base sampling frequency of 200 Hz is used, alternate samples being of the Lyman-alpha.

2.5) During sampling a real-time display of 1 s means is available. Since detailed analysis of the data is required, a means of storing the data is needed. Transferring the data straight to floppy disc in real-time would not be successful due to disk head-movement/settlement times. Therefore, extra RAM is fitted to the computer in the form of a 128 kilobyte sideways RAM. The data are transferred, in real-time, to the sideways RAM, in 5-minute blocks, each block then being copied to floppy disc for longer term storage and subsequent analysis.

3) THEORY OF OPERATION

In the following discussion:-

a subscript "1" indicates environmental quantities (ie. outside probe)

a subscript "2" indicates quantities at the source/detector.

Now $\rho \propto \frac{P}{T}$ .....(1)

where ρ is the air density at pressure, P(mb) and temperature, T(K).

Also, in a sample of air, total water content (q_t) is conserved and

$$q_t = \frac{\rho_v}{\rho} \quad .....(2)$$

where ρ_v is the water vapour density.

So, $$\frac{\rho_{v2}}{\rho_2} = \frac{\rho_{v1}}{\rho_1} .....(3)$$

$$\Rightarrow \rho_{v1} = \frac{\rho_1}{\rho_2} \rho_{v2} .....(4)$$

Since $$\frac{\rho_1 T_1}{P_1} = \frac{\rho_2 T_2}{P_2} .....(5)$$

Substituting for $\frac{\rho_1}{\rho_2}$ in equation (4) using (5) gives

$$\rho_{v1} = \frac{T_2 \cdot P_1}{T_1 \cdot P_2} \cdot \rho_{v2} \quad .....(6)$$

However, the theory of operation of the Lyman-alpha (Buck,1976) and the electronic design mean that ρ_{v2} and V_{out} are related by an expression of the form:-

$$\rho_{v2} = f(V_{out}) + C \quad .....(7)$$

where f is the calibration function.

V_{out} is the output voltage from the logarithmic amplifier

C is a constant related to the absolute intensity of the source illumination. In fixed-path operation this is related to window deterioration and source tube current (Buck,1985).

Substituting equation (7) in equation (6) gives:-

$$f(V_{out}) + C = \frac{T_1 \cdot P_2}{T_2 \cdot P_1} \cdot \rho_{v1} \quad .....(8)$$

This equation provides the basis for all the experimental tests carried out.

3.1) Calibration

Assume P_1 , P_2 and C are constant while ρ_{v1} is varied.

T_1 and T_2 are kept approximately constant.

V_{out} , T_1 , T_2 and ρ_{v1} (from a reference hygrometer) are measured.

With reference to equation (8),

Plotting V_{out} vs $\frac{P_2 \cdot T_1}{P_1 \cdot T_2} \cdot \rho_{v1}$ reveals the form of $f(V_{out})$.

3.2) Temperature sensitivity

Assume P_1 , P_2 , ρ_{v1} , T_1 are constant while T_2 is varied.
Measure T_1 , T_2 , ρ_{v1} (as above), V_{out}.

With reference to equation (8),

Plotting V_{out} vs $\frac{P_2 \cdot T_1}{P_1 \cdot T_2} \cdot \rho_{v1}$

should reveal the same calibration curve $f(V_{out})$ + C as in 3.1 above. Any deviation must imply some temperature sensitivity of the Lyman-alpha hygrometer.

3.3) Wind tunnel liquid water tests

As described in section 5.5 below, these were conducted in the wind tunnel by switching a known water spray on and off and measuring the change in the output voltage, V_{out}.
Assuming that P_1 , P_2 , T_1 , $f(V_{out})$ and C remain unaltered during the period over which the voltage change is detected (a few seconds) enables equation (8) to be differentiated to read:-

$$f'(V_{out}) \delta V_{out} = \frac{P_2 \cdot T_1}{P_1 \cdot T_2} \cdot \delta\rho_{v1} - \frac{P_2 \cdot T_1}{P_1 \cdot T_2} \cdot \rho_{v1} \cdot \frac{\delta T_2}{T_2} \quad \ldots\ldots\ldots (9)$$

where $f' = \partial f / \partial \rho_v$. Because of the self adjusting nature of the heaters and the small ratio of the energy supplied to latent heat of vaporisation compared to the total heater output, δT_2 is small (but see also below).

Then $$\frac{P_1 \cdot T_2}{P_2 \cdot T_1} \cdot f'(V_{out}) \cdot \delta V_{out} = \delta\rho_{v1} \quad \ldots\ldots\ldots (10)$$

which can be tested if P_1 , P_2 , T_1 , T_2 , δV_{out} and $\delta\rho_{v1}$ are measured and $f(V_{out})$ is known from (3.1).

For δT_2 to be small, $\rho_{v1} \cdot \frac{\delta T_2}{T_2} \ll \delta\rho_{v1}$

or $$\delta T_2 \ll \frac{\delta\rho_{v1} \cdot T_2}{\rho_{v1}} .$$

If the smallest $\delta\rho_{v1}$ measured is 0.1 g m^{-3} , $\rho_{v1} \sim$ 10 g m^{-3} at a maximum and $T_2 \sim$ 350 K, then equation (10) is sufficiently accurate if $\delta T_2 \ll$ 3.5 K. During the trials it was found that T_2 changed through less than 1°C on injecting water into the probe. Note that equation (9) does not depend on C ie. the source current (UV illumination) may be varied at will during the test to remain at an optimum setting if desired.

4) CALIBRATIONS

Calibrations were continued, as described in Met O 15 Internal Report No. 56 and as detailed in section 3.1 of this report, in a cold-room using a hygristor. However, to extend the range of water contents (ρ_v), 4 calibrations were conducted in an environmental chamber.

Fig. 6 shows a plot of all the calibrations made from the cold-room and the environmental chamber. All were made at the same value of I_{source}. However because they took place over an extended period of time, C was found to vary. Therefore C was determined by a least squares fit for each calibration and removed from the data plotted in Fig. 6. The calibration is approximately linear, as expected although a better fit is obtained with

$$f(V_{out}) = 0.85V_{out} + 1.12*10^{-2}V_{out}^2 \quad \text{.....(11)}$$

as shown in Fig.6

Differentiating this expression implies a change in sensitivity from 0.85 g $m^{-3}V^{-1}$ when ρ_v=0.0 g m^{-3} to 1.27 g $m^{-3}V^{-1}$ at ρ_v=20 g m^{-3}, a change by a factor of 1.49. According to Buck(1975) this quasi-linear calibration is a result of using the UH_3 source which is much more spectrally pure than a conventional discharge lamp. He also found a similar sensitivity change over the same range (1.5), but with a conventional source this increased to 2.9.

The steady variation in C is shown in Fig. 7 which, it is believed reflects the degradation in the magnesium fluoride windows of the source/detector tubes. According to Buck it is

partially reversible by cleaning.

TEMPERATURE SENSITIVITY

Varying the sample temperature as described in 3.2 above, produces a mean sensitivity of 0.86 +/- 0.03 g $m^{-3}V^{-1}$ over the range 2.5 - 4.5 g m^{-3} as shown in Fig. 8. This is not significantly different from the range of sensitivities derived from eqn.(11) over this range (0.87 - 0.90 g $m^{-3}V^{-1}$). Changing temperature does not appear to have changed the sensitivity by any significant amount and in aircraft use it is anticipated the sample temperature will only vary by a few K rather than the 30 K as in Fig. 8.

5.) WIND TUNNEL TESTS - 1ST. SERIES (Dec. '84, Mar. '85)

To ensure the probe would operate satisfactorily in aircraft use a series of wind-tunnel tests were performed using the Lucas Aerospace facilities at Artington.

The tunnel (Fig. 9 & 10) consists of a working section of 12 in^2 in cross-section by ~ 3 m long for speeds up to 100 m s^{-1}. The facilities included refrigeration (10 °C to -30 °C), water spray injection (up to 3 g m^{-3} with a mean drop radius of 10 microns) injected into the airstream by two nozzles ~ 3 m upstream of the working section and ice particle production (rotating blades on ice blocks giving particles of longest dimension between 0.5 and 4 mm , selectable, using sieves). All these facilities were used such that the probe was subjected to normal and extreme flying conditions.

The probe was mounted on a tunnel window such that its axis was along the tunnel axis as shown in Fig. 10. To cater for tests changing the angle of yaw, the mounting was capable of rotating a few degrees either side of this central position.

5.1) HEAT BUDGET

Because of the difficulties of making direct measurements of flow velocities within the probe inlet without disturbance, sampling volume and hence inlet velocity were calculated from a heat budget method.

Since:-

Power supplied to heaters (I) = Heat gained by sampled air (II) + Heat losses (III) ,

the volume flow through the probe can be found if the total power supplied to the heaters and the heat losses are known. Power supply to the heaters was therefore continuously measured and the heat loss characteristics were determined by wind tunnel tests. Altering the input power level and the temperature of the tunnel air and assuming that the inlet velocity was equal to the tunnel speed with the exhaust orifice open at 5 turns enables the heat loss to be calculated as a residual. This method was found to give good agreement in comparison with values deduced using a large capacity flowmeter (rotameter) in the laboratory. At 100 m s^{-1}, the heat loss was found to vary approximately linearly with (T_s-T_c) (where T_s= the sample temperature and T_c = the environmental temperature) as seen in Fig.11. Once this is known, the heat budget can be used to derive the inlet velocity. Although the method does not provide an absolute calibration, a

measure of its success can be seen in Fig.12 which shows the values derived for many runs at a nominal 100 m s^{-1} tunnel velocity.

At a tunnel temperature of 0°C and an airspeed of 100 m s^{-1}, the balance is approximately

1200 = 700 + 500 (all quantities in W)
(I) (II) (III)

ie. a +/- 50 W m^{-2} uncertainty in (II) leads to a +/- 7% uncertainty in volume flow rate and inlet velocity. However, the relative accuracy (over small changes of temperature and power input) should be much better than this. The correction required by the additional heat needed to evaporate water drops when water was injected was approximately 20x W where x is the liquid water content in g m^{-3}. This is generally small compared with the other uncertainties and is virtually undetectable.

The heat budget can also be used to predict the sample temperature as a function of inlet temperature. At 100 m s^{-1}, the power drawn by the heaters, H, is given approximately by the function shown in Fig.13. The limiting value of H as T_c decreases reflects the limitations of the heating elements (rated at 500 W maximum each) and the supply transformer which could not maintain higher power levels. Using the heat loss curve defined in Fig.11 and knowing the volumetric flow rate enables an expression for the sample temperature to be derived:-

$$T_s=0.44T_c-0.011(T_c)^2+79 \ (^oC).....(12)$$

This is shown in Fig.14 together with the observed values which agree well. Note that if the expressions for heat input and loss are only accurate to within +/- 50 W m^{-2}, the temperature

difference (T_s-T_c) is only predicted to within about +/- 10% ie. the uncertainties in T_s from equation (12) are ~ +/- 8 K, although again over a small range of T_c, the relative accuracy should be much better.

5.2) ISOKINETIC SAMPLING

As mentioned previously, the flow through the probe can be calculated using a heat budget method. The tunnel was run up to 102 m s^{-1}, measured by independent pitot-static pressure tube. The exhaust deflector gap was then adjusted along its screw thread and heat budget velocities calculated. The response of the calculated inlet velocity was as shown in Fig.15a. Sampling appears to be isokinetic within a few percent when the exhaust deflector is set at least 5 turns along its screw thread from the fully closed position. This value was used throughout all the subsequent trials.

5.3)YAW ANGLE SENSITIVITY

The probe was also adjusted for yaw and heat budget velocities calculated. Fig.15b shows that the probe is sensitive to angle of yaw, however, in normal use, changes in angle of yaw and angle of attack do not usually exceed 2^o during an experimental run which corresponds to a 3% change in nozzle airspeed. Of course, the primary measurement (specific humidity) should not be sensitive to small airspeed changes.

5.4)LYMAN-ALPHA NOISE LEVELS

During runs in the wind-tunnel it was apparent that the noise level on the hygrometer output rose from 0.05 V whilst the tunnel was at rest to a maximum of ~ +/- 0.1 V (~ +/- 0.1 g m^{-3}) when the tunnel was run up to speed. This was believed to be due to vibrations transmitted to the probe from the wind tunnel itself. Fast Fourier transform spectral analysis of the Lyman-alpha output showed this tunnel induced noise to be of no particular frequency. The most likely source was thought to be the signal cable from the detector to the first amplifier although this was of shielded coax. ~ 5 cm long, fixed along its length. (See later for further modifications.)

5.5)WATER AND ICE INJECTION EXPERIMENTS

Tests using a Particle Measuring Systems ASSP-100 showed the droplet spray issuing from the tunnel spray nozzles to be of a uniform nature with a mean radius of 10 microns. The spray nozzles were calibrated using the standard method of placing a metal bar which had been previously cooled below 0 ^oC, into the tunnel with the spray nozzles on for a known period. The build up of ice on the metal bar was then measured and converted to a liquid water content for that setting of the spray nozzles.
The experiments consisted of operating the instrument at wind tunnel airspeeds of 100 m s^{-1} and spraying water and ice at different water and ice contents over differing lengths of time. Initially, water was sprayed for short periods of about 10 s. A typical example of the Lyman-alpha response is shown in Fig.16. Results such as these showed that although the instrument was at

least capable of responding to the ramp change when the spray was turned on (which probably took ~1 s), it took several seconds to recover following switch off (marked C in Fig.16), suggesting that some water was still retained within the instrument, upstream of the detector for several seconds. The recovery period (marked C in Fig.16) was a minimum of ~2 s with 0.1 g m^{-3} and increased to 5 s with 2 g m^{-3} of liquid water.

Referring to Fig.16, from each OFF/ON/OFF period an estimate of the water vapour detected by the probe was made by taking a 5 s average output voltage just before the water/ice was detected (marked A), a 5 s average after the water/ice was no longer detected (marked D) and averaging these two figures to give a mean baseline. An average was also calculated over the whole period when steady water/ice injection was detected (marked B). From these two means a voltage difference was calculated which was related to the change in humidity mixing ratio, ρ_v, using equation (10) and (11). A comparison of the injected liquid/ice content vs. the detected contents is shown in Fig. 17.
Although the results agree at low liquid water values (</= 0.5 g m^{-3}), the higher values are progressively under-estimated and highly scattered. This is clearly related to the problem of liquid water retention as discussed above.

The instrument was also subjected to long runs of continuous water and ice input over a range of water/ice contents. It was found especially with water contents > 0.5 g kg^{-1}, that broad spikes (Fig.18) appeared on the detector output a few minutes after the start of water injection and for some tens of seconds after water injection had ceased. These spikes are characteristic

of large mm sized drops passing through the instrument (eg. see Met.0.15 Internal Report 56). The water injection system was not suspected as its output was of a very uniform nature and could be shut off in a few seconds. On inspection of the inside of the nozzle, significant amounts of water were found adhering to the wall. This suggests that water was collecting on the inside surface of the nozzle and occasionally being dislodged to pass through the instrument. A wire support for a thermistor mounted across the diameter of the intake would also assist any water collection and subsequent shedding. The gradual build-up of liquid on the inner walls of the intake nozzle, eventually leading to large droplets being shed into the evaporator after a few minutes can explain all the problems encountered above: the residual signal when the water was switched off and its dependence on liquid water content, the appearance of the large spikes after a few minutes operation at higher liquid water levels and their continuation after the spray was extinguished and the poor agreement seen in Fig.17.
Finally, although the instrument had been initially designed to operate in non-freezing conditions, the opportunity was taken to investigate its characteristics during icing conditions.

Visually, icing was evident on the nose-cone whilst temperatures were below freezing, the rate of icing being dependent on the liquid water/ice content of the air and the air temperature. In severe icing conditions (T=-15°C, q_l=2 g kg^{-1}), ice grew forward of the nozzle tip, tending to close the nozzle and reducing air-flow into the probe. Fig.19 shows the icing on the instrument after a run at -5°C, and a liquid water content of 1.0 g m^{-3}.

6.) MODIFICATIONS AFTER 1st. WIND TUNNEL TRIALS

To overcome the problems discussed above a number of modifications were carried out. The first three changes listed below were designed to reduce the possibility of water collecting and shedding upstream of the heater assembly.

1) In an effort to provide some nozzle tip de-icing and to eliminate water collecting on the inside of the nozzle, the inside wall of the nozzle was heated. This was achieved by redesigning the nose cone as shown in Fig.1. The previously solid metal cone was machined away to leave the inner wall as thin as possible. Three nichrome heaters were wound tightly around the nose cone over a ceramic insulating layer to give an even distribution of heat along the length of the nose cone. The cone was then cast in thermally insulating 'Araldite' to recover the original exterior shape. The heaters were controlled using bridge circuits such that the power to each could be controlled independently. Also embedded in the wall of the nose cone were three thermistors so that the wall temperature could be monitored and recorded.

2) The thermistor upstream of the evaporator was moved outside the probe altogether and placed on the pylon connecting the probe body to the wind-tunnel window. This thermistor measures the ambient air temperature so its precise location is unimportant provided it remains correctly exposed.

3) Internal joints, especially upstream of the evaporator, were kept to a minimum by inserting a P.T.F.E. sleeve which was in

contact with the front of the evaporator leaving only one joint upstream of the heaters. This joint was carefully profiled to discourage the accumulation of water.

4) A static rotor was placed between two of the stainless steel screens. This serves to increase turbulent mixing of air within the probe prior to sampling by the hygrometer and reduces the possibility of hygrometer sampling bias due to any tendency for large drops to pass through the evaporator close to the central probe axis. Tests using a large capacity flow meter showed this not to affect the rate of flow through the probe.

7.) WIND TUNNEL TESTS - 2ND SERIES (June '85)

7.1) HEATED NOZZLE

First, the modified nose cone was tested at an airspeed of 100 m s^{-1} and a temperature of 15°C, the thermistors measured 53°C (front), 90°C (middle) and 46°C (rear) with a total power input of 300 W. These temperatures were maintained to within ~20°C for the remainder of the experiments. At -7°C, temperatures of 55°C (front), 74°C (middle) and 27°C (rear) were recorded with a total input of 300 W to the heaters. Of course, whilst the heaters are on, the heat budget velocity calculations will not be valid due to the additional heating of the sampled air.

7.2) WATER INJECTION

The water injection tests carried out in the first series of wind-tunnel tests were repeated. Figs.20-22 show equivalent

results to those plotted from the original tests in Figs.16-18. Note that there is no long recovery period after switching off the spray (Fig.20). Some structure is observed on switch off which probably reflects the time taken to turn off the sprays completely which is considerably longer than the rise time on switching on. Note also that the large spikes are absent during and after the water injection - even on long runs (~5 minutes, Fig.21). Rapid dismantling (although taking longer than removal of the original nozzle, 60 s cf. 10 s) revealed a completely dry internal surface. Finally, the agreement between the probe liquid water contents and those derived independently from the icing spray are very good (Fig.22) even at very high liquid water contents.

In icing sprays, the additional nose heating was also found to de-ice the nozzle tip quite successfully and no build-up of ice on the tip in severe icing conditions was evident.

8.)VIBRATION TESTS

Following the wind-tunnel tests when noise on the Lyman-alpha output due to vibration of the probe was detected, vibration tests were carried out on the Met.0.16 vibration table at the Eastern Road site.

The vibration equipment consisted of a transducer, accelerometer, power amplifier and control centre. The control centre was capable of controlling the transducer under two main modes:-

1) Automatic frequency sweep with constant displacement, peak velocity or acceleration.
2) Manual control of frequency and displacement, peak

velocity or acceleration.

The complete probe (Fig.1) was securely attached to the vibration table and the experiment consisted of imparting vibrations to the probe at fixed frequencies for several fixed displacements. The frequencies, displacements and resultant accelerations used, were chosen with reference to tests performed on a HC-130C by Lockheed (ref.4) and on the M.R.F. C-130 (ref.5). The main driving frequencies detected on these aircraft are found at 68 Hz (the predominant propeller blade passing frequency) and at 178 Hz The frequencies chosen for the tests encompass both these frequencies and the accelerations imparted exceed those expected when the probe is mounted on the aircraft. For example, from the tests on the cargo floor of the HC-C130H (ref.4), accelerations of the order of +/- 0.3 g (ie. amplitudes of 0.0127 mm) were encountered at 68 Hz whilst these tests used accelerations up to +/- 2.6 g (amplitudes of 0.25 mm) at this frequency.

Data was recorded on the microcomputer as before but at a frequency of 1280 Hz. This higher frequency was chosen so that the noise frequencies could be adequately resolved.

An example of a Fast Fourier Transform from 0.2 s of Lyman-alpha detector data is shown in Fig.23. In this example, as in all the other runs, the dominant noise on the Lyman-alpha output occurs at the vibration table driving frequency (120 Hz in this case).

At each table vibration frequency, a 0.2 s period of Lyman-alpha data was selected, Fast Fourier Transformed and the amplitude of the peak spectral estimate recorded (Zmax in Fig.23) together with the peak-to-peak amplitude of the table vibration. These data were then plotted as shown in Fig.24. This shows, that with increasing amplitude (plotted symbol increasing from A to M) the noise induced on the Lyman-alpha output also increases. The noise

amplitude also increases with increasing frequency up to a peak at around 190 Hz.

As mentioned above the expected aircraft vibrational peak-to-peak amplitudes at these frequencies is of the order of 0.0127 mm which corresponds to amplitudes less than that denoted by symbol (A) in Fig.24.

The highest peak-to-peak noise level on the Lyman alpha output was observed at 190 Hz (denoted 100% in Fig.24), which is equivalent to +/- 1.5 V. The most likely source of this noise is vibration of the co-ax. cable which connects the detector and the pre-amp. The very small signals produced by the detector and the consequent high gain of the pre-amp. make the device very sensitive to small disturbances of the cable.

A new detector pre-amplifier configuration was then installed in which the pre-amplifier assembly was miniaturised and mounted directly on the output pins of the detector, thus reducing the possibility of noise pick-up.

The probe was then subjected to the same tests as before. The results are shown in Fig.25. Note the expansion of the amplitude axis on the left. At the critical frequencies of 68 and 178 Hz, the resultant noise has been considerably reduced by at least a factor of 5 (68 Hz) and 48 (178 Hz). At amplitudes believed to be typical of the C130 (0.0127 mm at 68 Hz) this corresponds to a peak-to-peak noise level of +/- 0.025 V, or about +/- 0.02 g m^{-3}, a factor ~5 better than was observed in the wind tunnel trials (cf. Figs.16, 18, 21). The peak found above 200 Hz is of little consequence since, on the aircraft, the hygrometer response will be recorded at a maximum frequency of 64 Hz so higher frequencies can be filtered out.

CONCLUSION

A prototype total water content probe has been designed and manufactured. A series of laboratory trials and two full tests in an icing wind tunnel at aircraft speeds has shown:

1) Mechanical design is strong, allows close approximation to isokinetic sampling and has sufficient throughflow to enable fast response measurements to be made.
2) A Lyman-alpha detector has been constructed which has a mainly linear and repeatable calibration. Noise levels are low and there appears to be little temperature sensitivity.
3) The Lyman-alpha source/detector is capable of working in conditions ~100°C for extended periods and repeated cycling to room temperature and back causes no apparent problems.
4) Following a series of modifications, notably, heating nozzle walls, good agreement between measured water input and tunnel calibration were obtained, even at very high liquid water contents.
5) As far as can be ascertained, the response time appears to be adequate for the intended aircraft use (see also ref. 6).
6) Repositioning the pre-amp. significantly reduced vibration-induced noise to acceptable levels.

Following this succesful outcome from this series of tests, it is considered that the current design has been sufficiently proven to form the basis for an aircraft-compatible instrument.

ACKNOWLEDGEMENTS

We would like to thank Mr.P.R.A.Brown for help with the data acquisition software, Mr.W.Wright and Met.O.16 workshops for their help during the construction of the prototype and to the staff of Lucas Aerospace wind tunnel facilities at Artington.

REFERENCES

1)Buck,A.L. 1976 The variable-path Lyman-alpha hygrometer and its operating characteristics. Bulletin American Meteorological Society, 57.9, 1113-1118

2)Buck,A.L. 1978 Notes on the fabrication of a fixed-path Lyman-alpha hygrometer. Research Systems Facility, NCAR, Boulder, Colorado.

3)Buck,A.L. 1985 The Lyman-alpha absorption hygrometer, NCAR, Boulder, Colorado

4) HC-130H Noise and vibration test report, Lockheed-Georgia Co.,Report no. ER-6707, April 6, 1966. Contract No. AF33(657)-12563.

5) Hercules XV208 Note on flight measurements of vibration in the fuselage. Stress Office, RAE Farnborough. Ref. LST/177/01. 29/3/79

6)Leighton,J.R.,1984 Total water content hygrometer: Design and Nicholls,S. calibration. Met.O.15 Internal Report No. 56

Figure Captions

Fig.1 Cross-section of Lyman-alpha total water content hygrometer, wind tunnel version (Dec.'85).

Fig.2 Hygrometer side-view.

Fig.3 Conventional nitric oxide photo-ionization chamber.

Fig.4 Low hydrogen pressure discharge lamp used as a U.V. source.

Fig.5 Schematic of the electronics.

Fig.6 Calibration data from 8 calibrations with a second order fit of:- $Rho=1.12*10^{-2}V^2+0.85V$ (g m^{-3})

Fig.7 Variation in C with time. C reflects the degradation of the magnesium fluoride windows of the source/detector.

Fig.8 Data plotted with differing sample temperatures (plotted nos.) to show unappreciable sensitivity of the hygrometer to temperature change.

Fig.9 Wind tunnel facilities used during the trials.

Fig.10 Detail of the wind tunnel (schematic).

Fig.11 Linearity of the heat loss from the probe at 100 m s^{-1}. Also plotted is the theoretical straight line with no heat loss.

Fig.12 Heat budget velocities calculated using a calculated heat loss at 100 m s^{-1} wind tunnel airspeed.

Fig.13 At 100 m s^{-1} the power drawn by the heaters was as shown by the (+). The function $H=1300-0.17(T_c+25)^2$ W. best describes these data.

Fig.14 Using the heat loss function defined in Fig.11 and knowing the volumetric flow rate through the instrument allows an expression for the sample temperature (T_s) to be derived:- $T_s=0.44T_c-0.011(T_c)^2+79$ (^oC) where T_c is the cold

(ambient) temperature. The plotted points show values obtained during wind tunnel runs, and give a fairly good agreement to the derived curve.

Fig.15a Nozzle airspeeds calculated using a heat budget method compared with exhaust deflector distance along exhaust port screw thread. Calculated velocities are shown to be close to the wind tunnel airspeed of 102 m s^{-1} at around 5 turns along the screw thread.

Fig.15b Nozzle airspeeds calculated using a heat budget method compared with angle of yaw of the instrument to the wind tunnel axis.

Fig.16 An example of the output of the hygrometer on injection of 1.0 g m^{-3} of water spray in the instruments original configuration. Note the recovery time (labelled C) and compare with Fig.20.

Fig.17 Comparison of tunnel calibrated liquid water content with Lyman-alpha derived liquid water content. Note the poor agreement and the general spread of the data.

Fig.18 Trace at the end of a 'long' run of injected water spray of 1.0 g m^{-3}. Note the spikes after water injection has been switched off and compare with Fig.21.

Fig.19 Two views of the probe after a water injection of 2.0 g m^{-3} at an air temperature of $-15^{o}C$. Just visible in the top view is ice growing forward of the nozzle tip.

Fig.20 A typical trace of the hygrometer output with nose cone inner wall and tip heating. Compare with Fig.16 and notice the reduced recovery time at water injection switch-off.

Fig.21 Similar to Fig.18 but with nose cone heating etc.

Fig.22 As Fig.17 but with heated nose cone etc. Note the good agreement of the mean values and the smaller dispersion.

Fig.23 An example of a Fast Fourier Transform on 0.2 s of hygrometer output recorded at 1280 Hz with a vibration table driving frequency of 120 Hz and peak-to-peak amplitude of 0.076 mm.

Fig.24 With the hygrometer pre-amp. in its original configuration this shows results from all the Fast Fourier analyses with the symbols (A to M) indicating vibration table peak-to-peak amplitude. The amplitude of each point is calculated from the Fast Fourier Transforms (see Fig.23), at the peak spectral estimate.

Fig.25 As Fig.24 but with the hygrometer pre-amp. in its new configuration. Notice the expansion of the left-hand axis.

Lyman-Alpha Total water Hygrometer

Fig.1

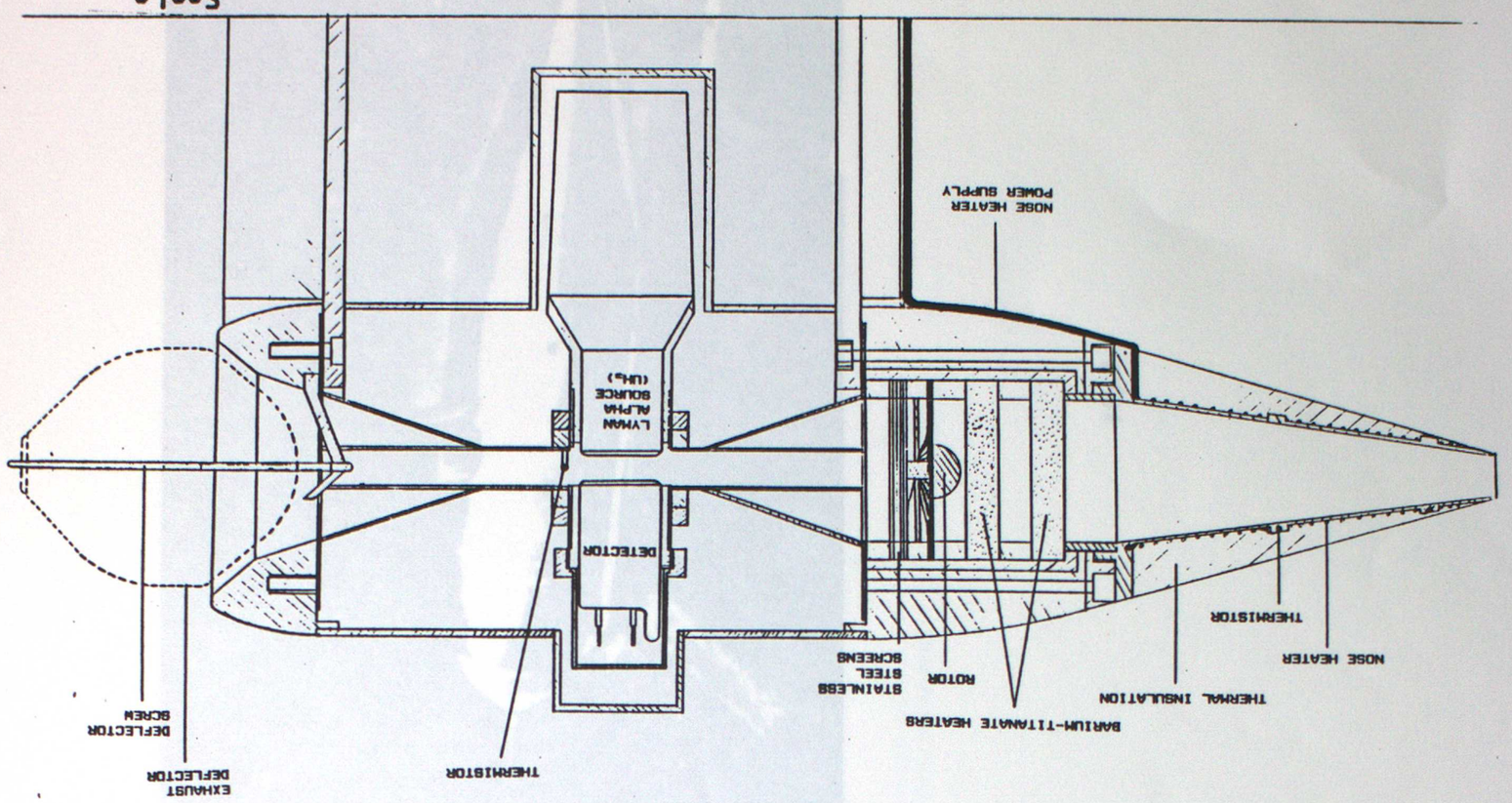

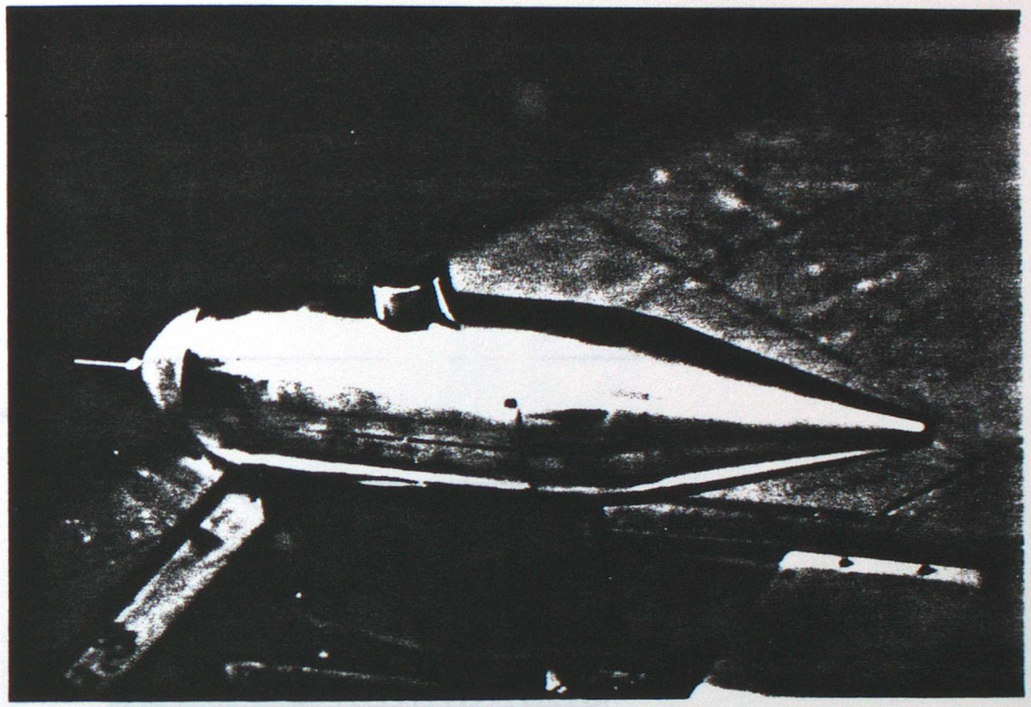

Fig.2

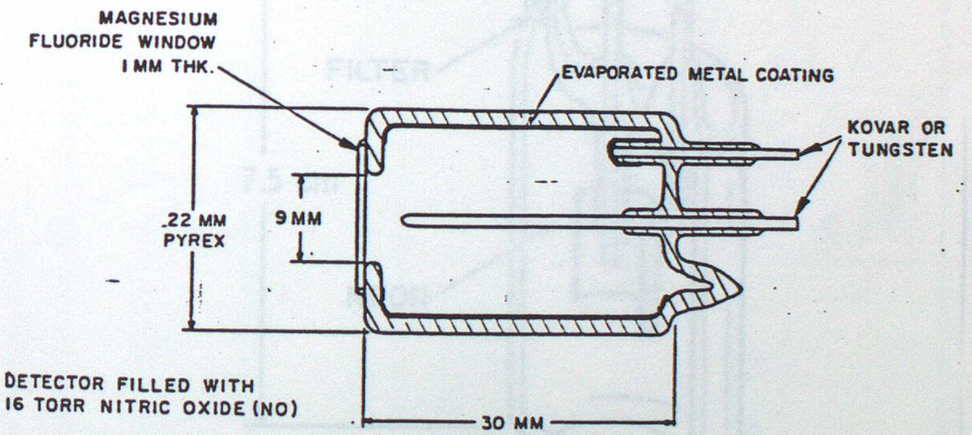
MAGNESIUM
FLUORIDE WINDOW
1 MM THK.
EVAPORATED METAL COATING
KOVAR OR
TUNGSTEN
.22 MM
PYREX
9 MM
DETECTOR FILLED WITH
16 TORR NITRIC OXIDE (NO)
30 MM

Fig.3

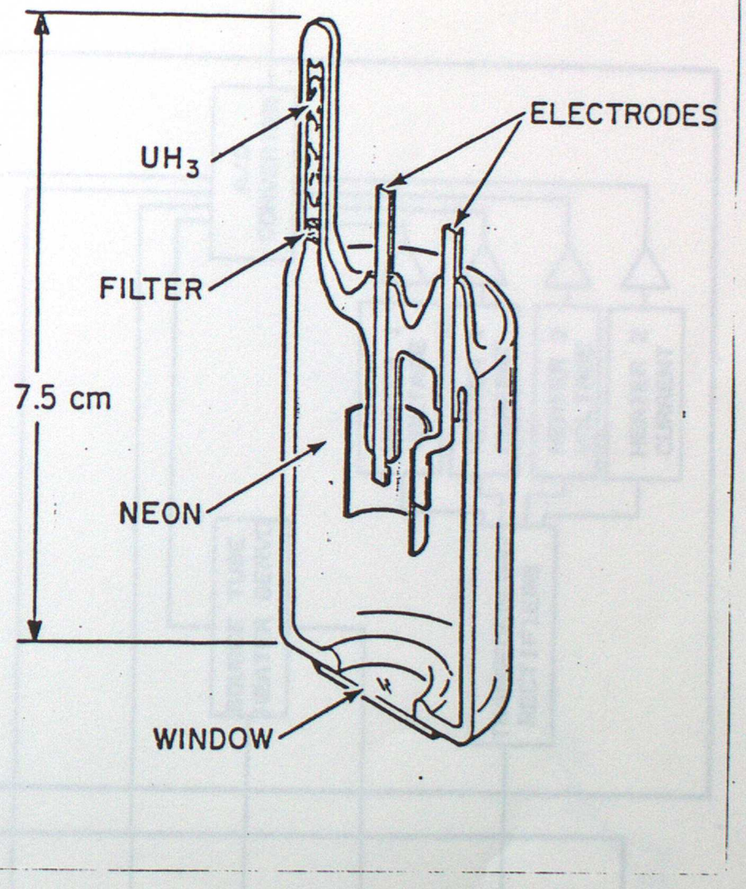

Fig.4

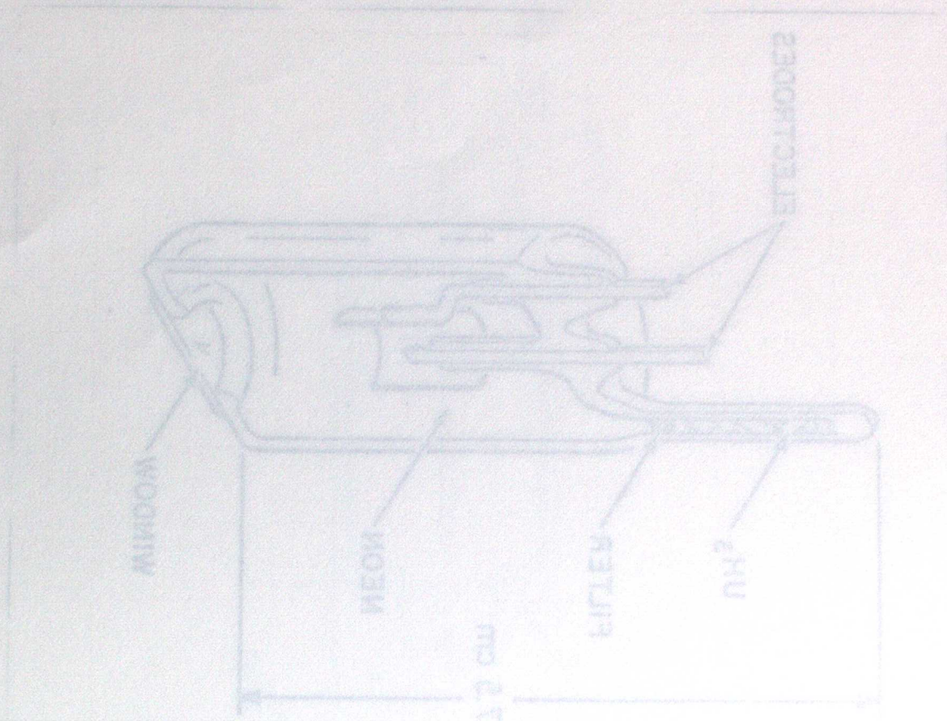
PROBE
DATA ACQUISITION
DATA STORAGE
DETECTOR
SAMPLE THERMISTOR
AMBIENT THERMISTOR
SOURCE TUBE THERMISTOR
SOURCE TUBE OVERHEAT THERMISTOR
EVAPORATOR HEATERS
SOURCE TUBE HEATER SERVO
TRANSFORMERS/ RECTIFIERS
HEATER 1 VOLTAGE
HEATER 1 CURRENT
HEATER 2 VOLTAGE
HEATER 2 CURRENT
A/D CONVERTER
VDU
MICRO
DISC

Fig.5

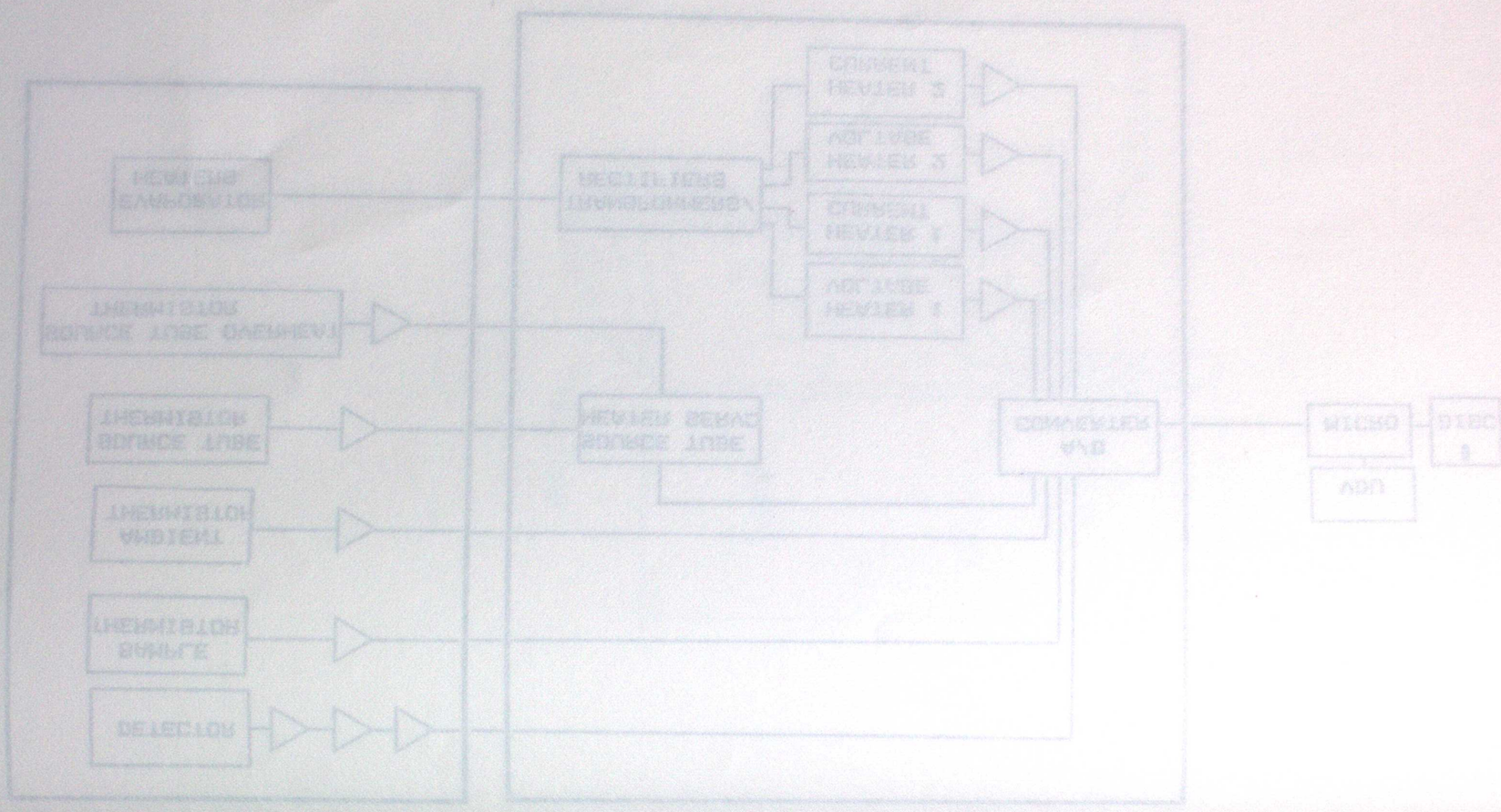

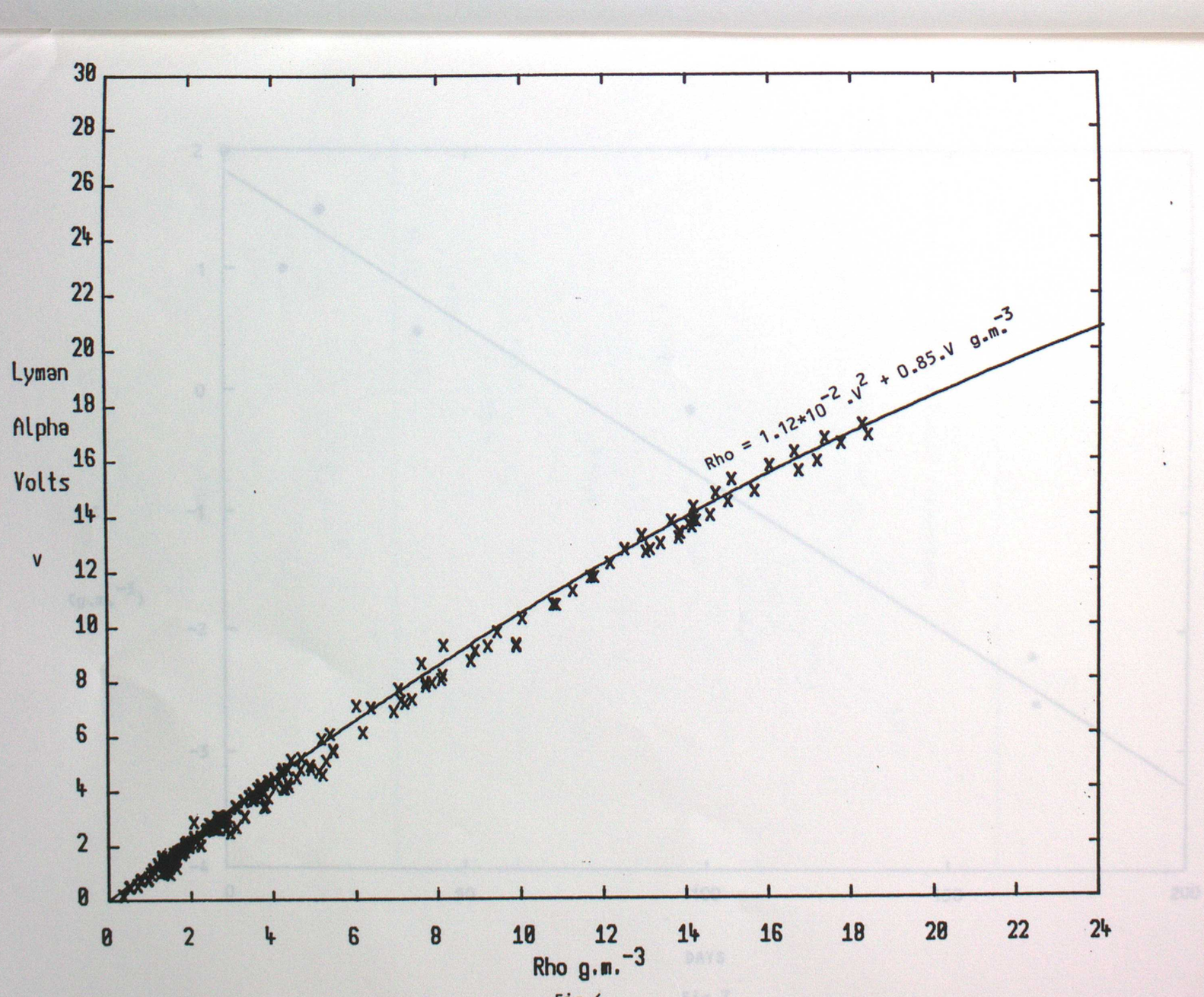
Lyman
Alpha
Volts
V
Rho = 1.12*10^-2 .V^2 + 0.85.V g.m.^-3
Rho g.m.^-3
0
2
4
6
8
10
12
14
16
18
20
22
24
26
28
30

Fig.6

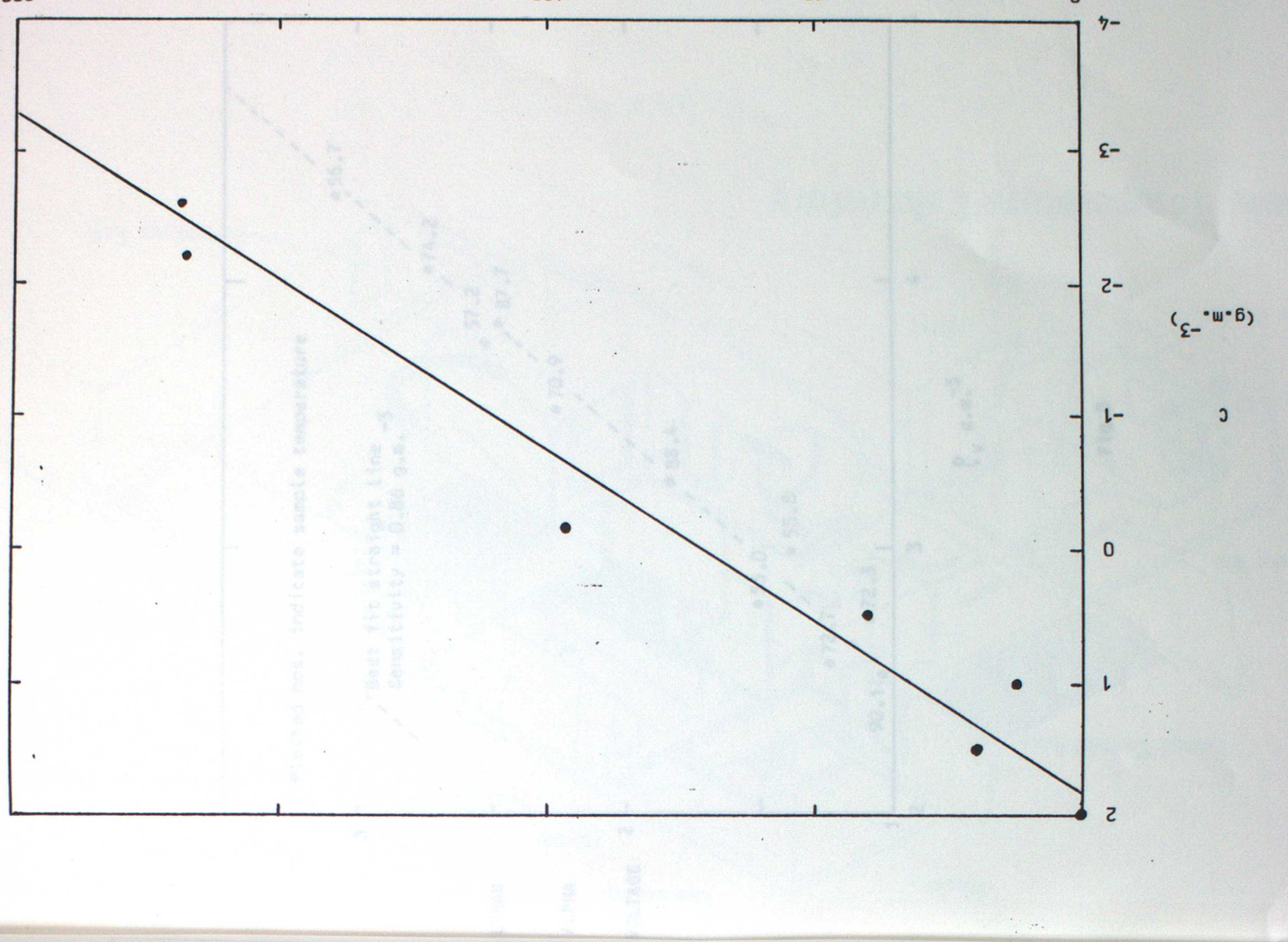

Fig.7

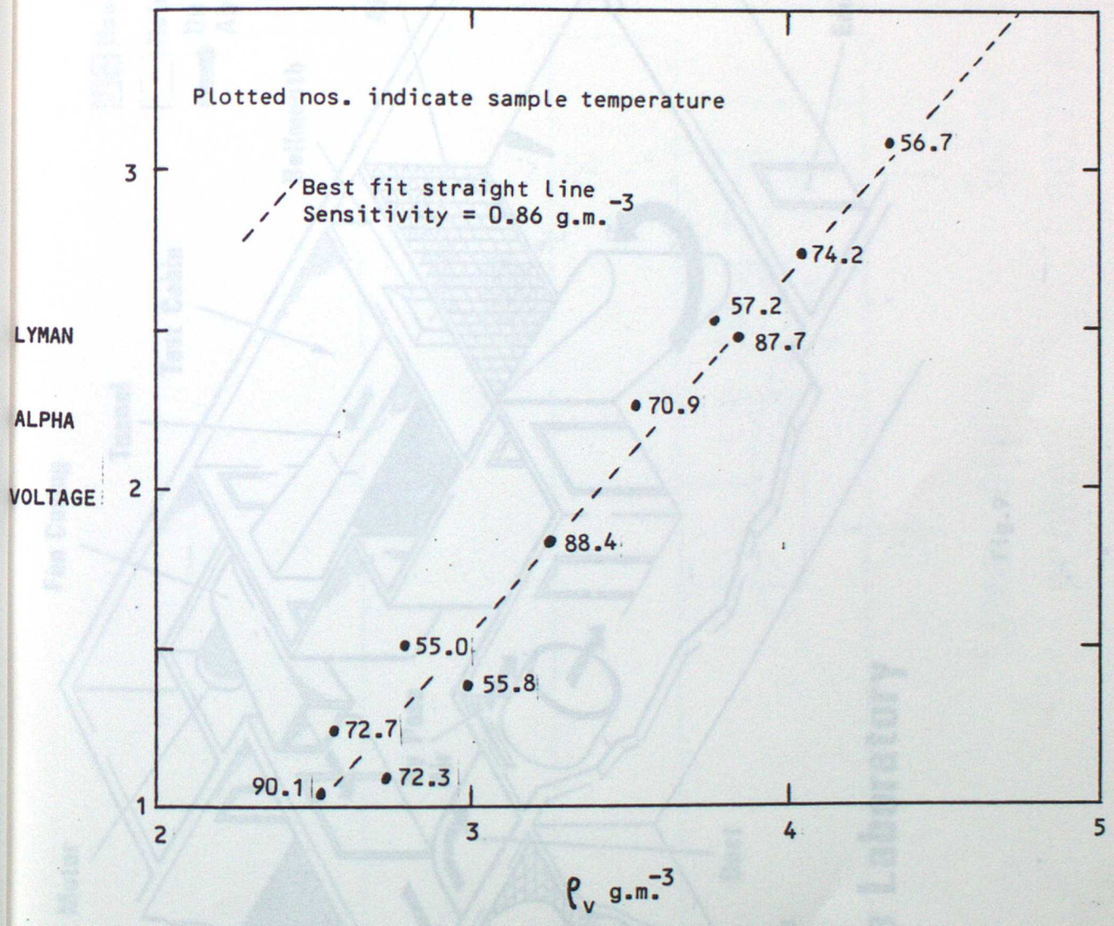
Plotted nos. indicate sample temperature
Best fit straight line
Sensitivity = 0.86 g.m.-3
56.7
74.2
57.2
87.7
70.9
88.4
55.0
55.8
72.7
72.3
90.1
LYMAN ALPHA VOLTAGE
3
2
1
2
3
4
5
ρv g.m.-3

Fig.8

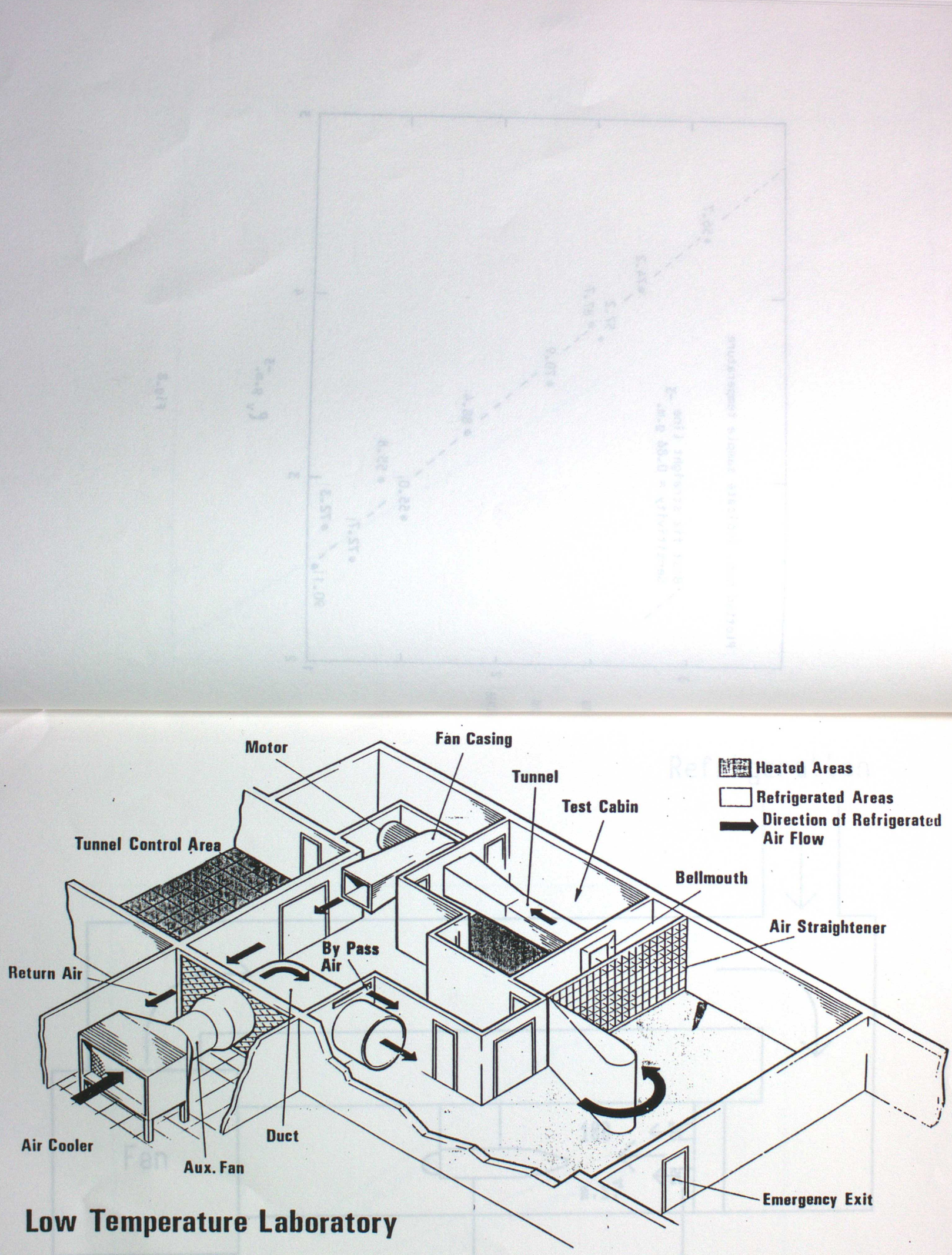
Motor
Fan Casing
Tunnel
Test Cabin
Heated Areas
Refrigerated Areas
Direction of Refrigerated Air Flow
Tunnel Control Area
Bellmouth
Air Straightener
By Pass Air
Return Air
Air Cooler
Aux. Fan
Duct
Emergency Exit
Low Temperature Laboratory

Fig.9

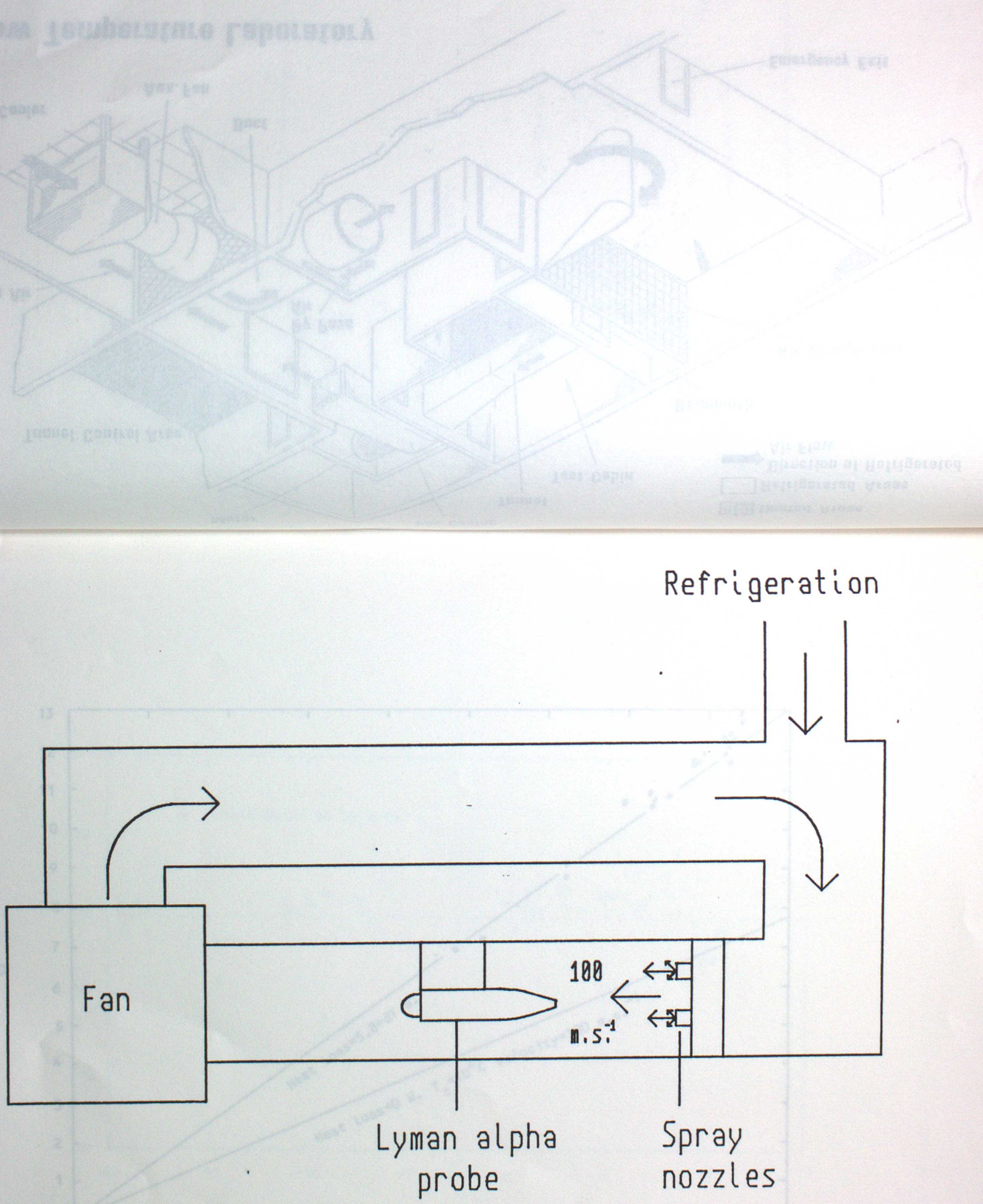

Wind tunnel configuration (schematic)

Fig.10

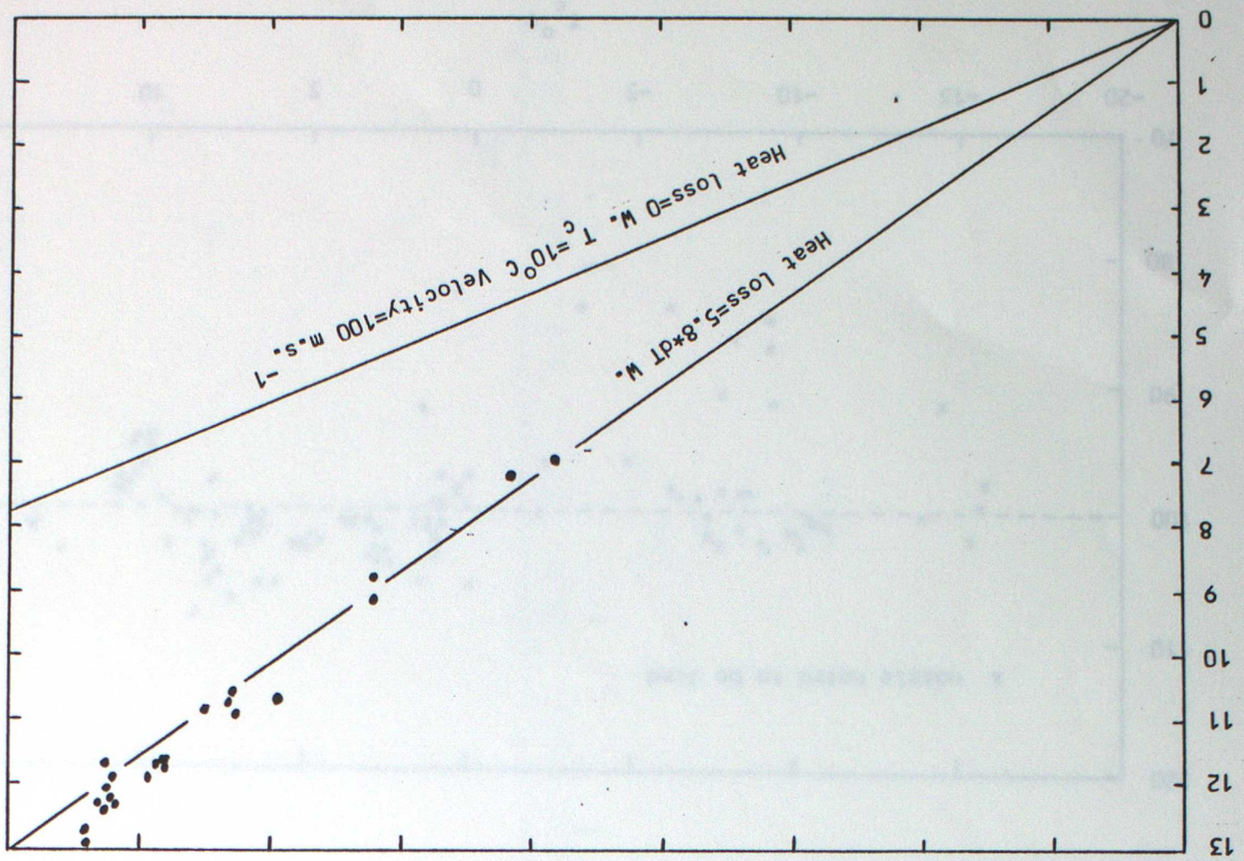
HEAT
INPUT
WATTS x 100
0
1
2
3
4
5
6
7
8
9
10
11
12
13
Heat Loss=5.8*dT W.
Heat Loss=0 W. T_c=10°C Velocity=100 m.s.-1
0
10
20
30
40
50
60
70
80
90
dT = T_s - T_c (°C)

Fig.11

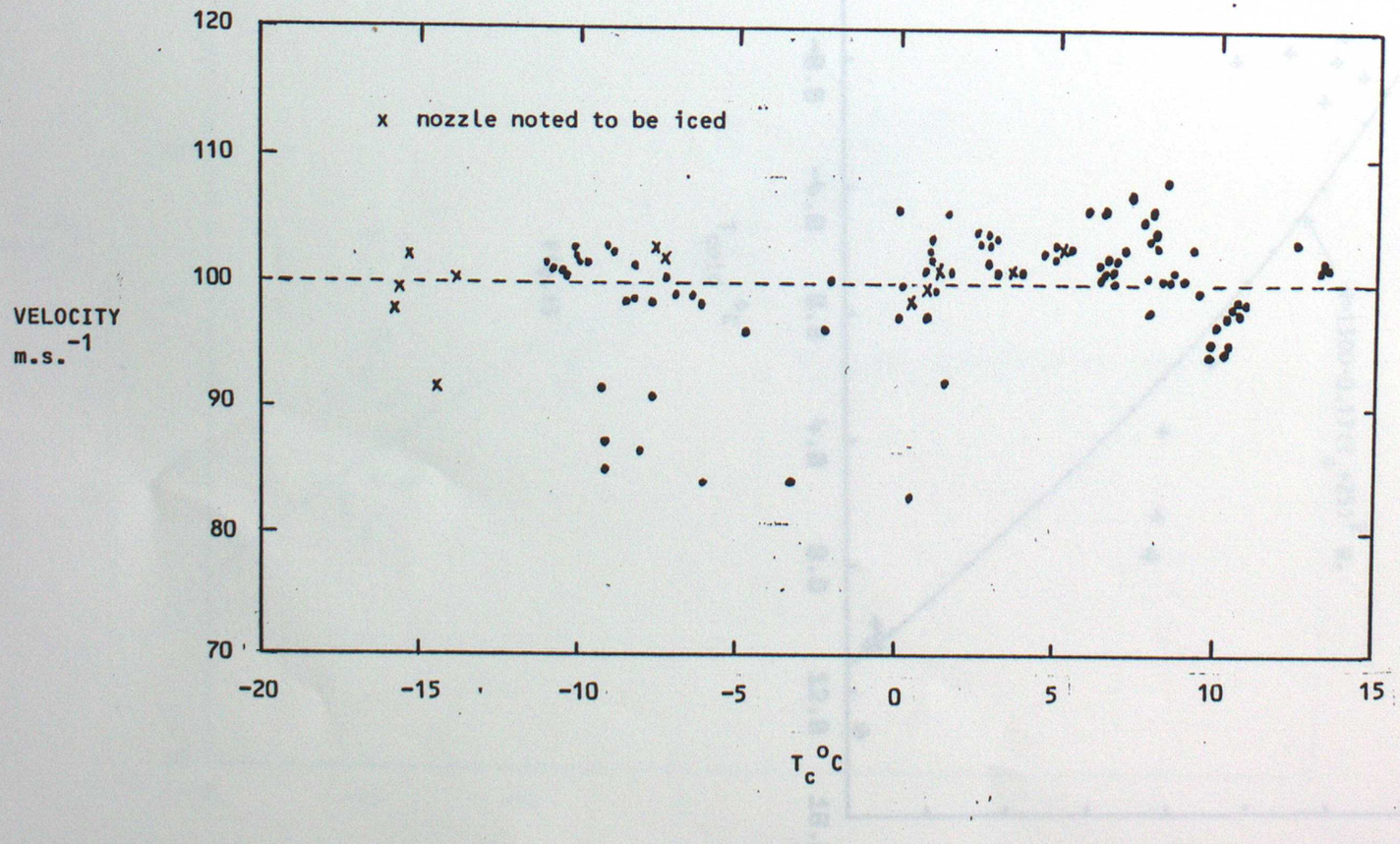
x nozzle noted to be iced
120
110
100
90
80
70
-20
-15
-10
-5
0
5
10
15
VELOCITY
m.s.-1
T_c °C

Fig.12

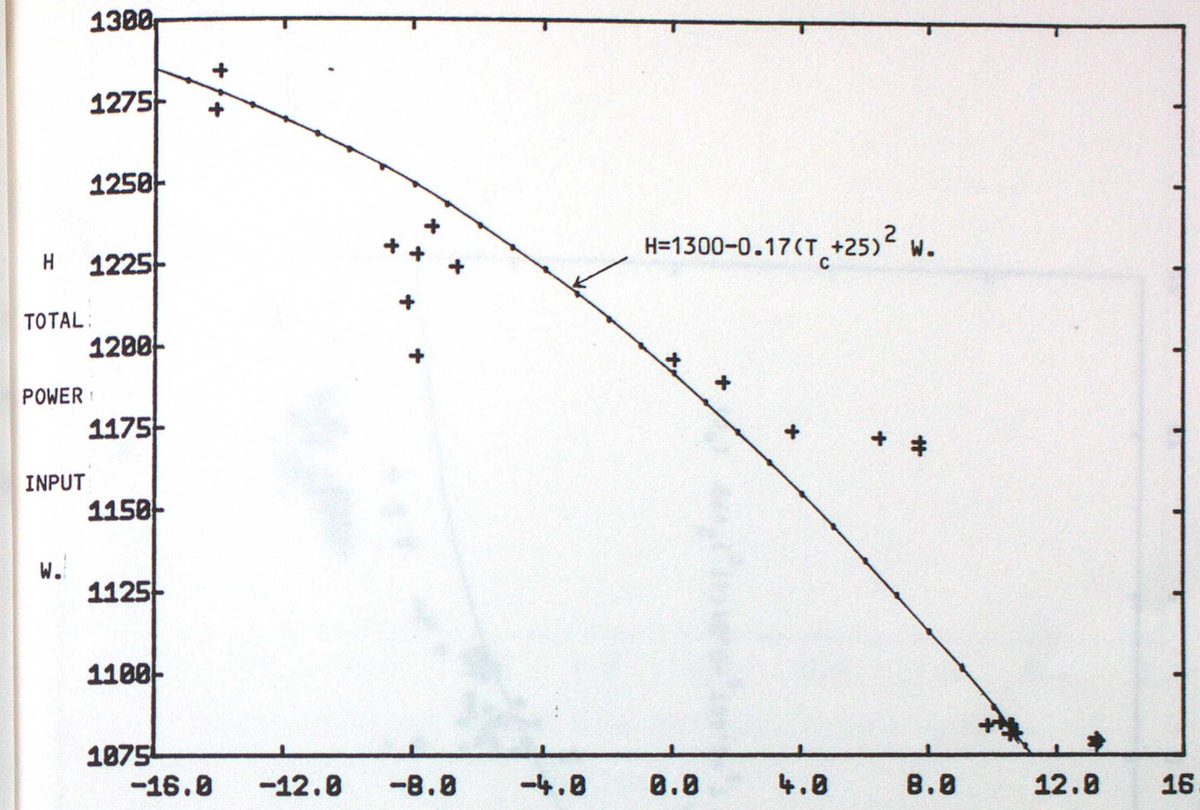
1300
1275
1250
1225
1200
1175
1150
1125
1100
1075
H
TOTAL
POWER
INPUT
W.
H=1300-0.17(T_c+25)^2 W.
-16.0
-12.0
-8.0
-4.0
0.0
4.0
8.0
12.0
16.0
T_cold °C

Fig.13

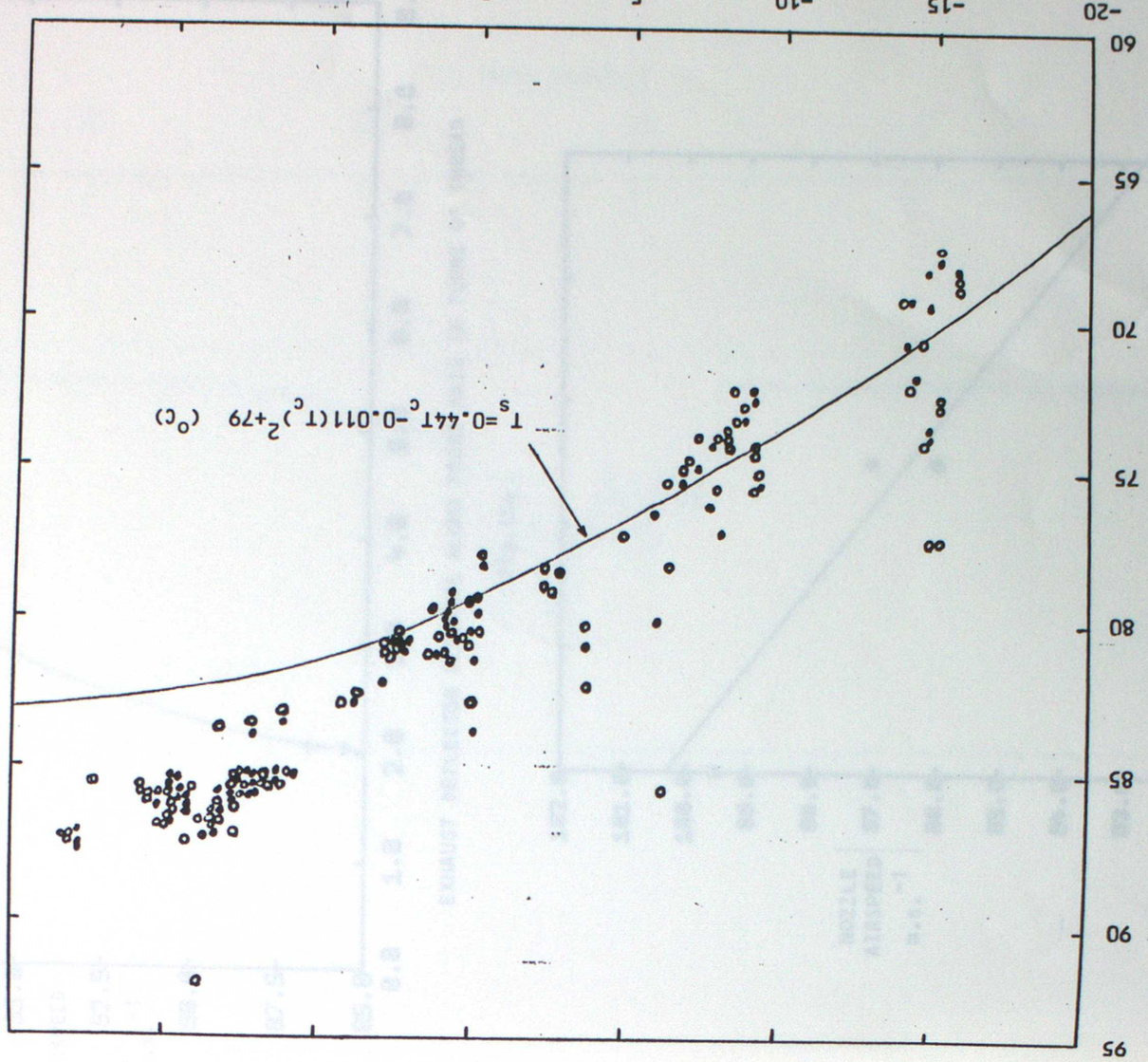
T_{sample} °C
95
90
85
80
75
70
65
60
-20
-15
-10
-5
0
5
10
15
T_{cold} °C
$T_s=0.44T_c-0.011(T_c)^2+79$ (°C)
water off
water on

Fig.14

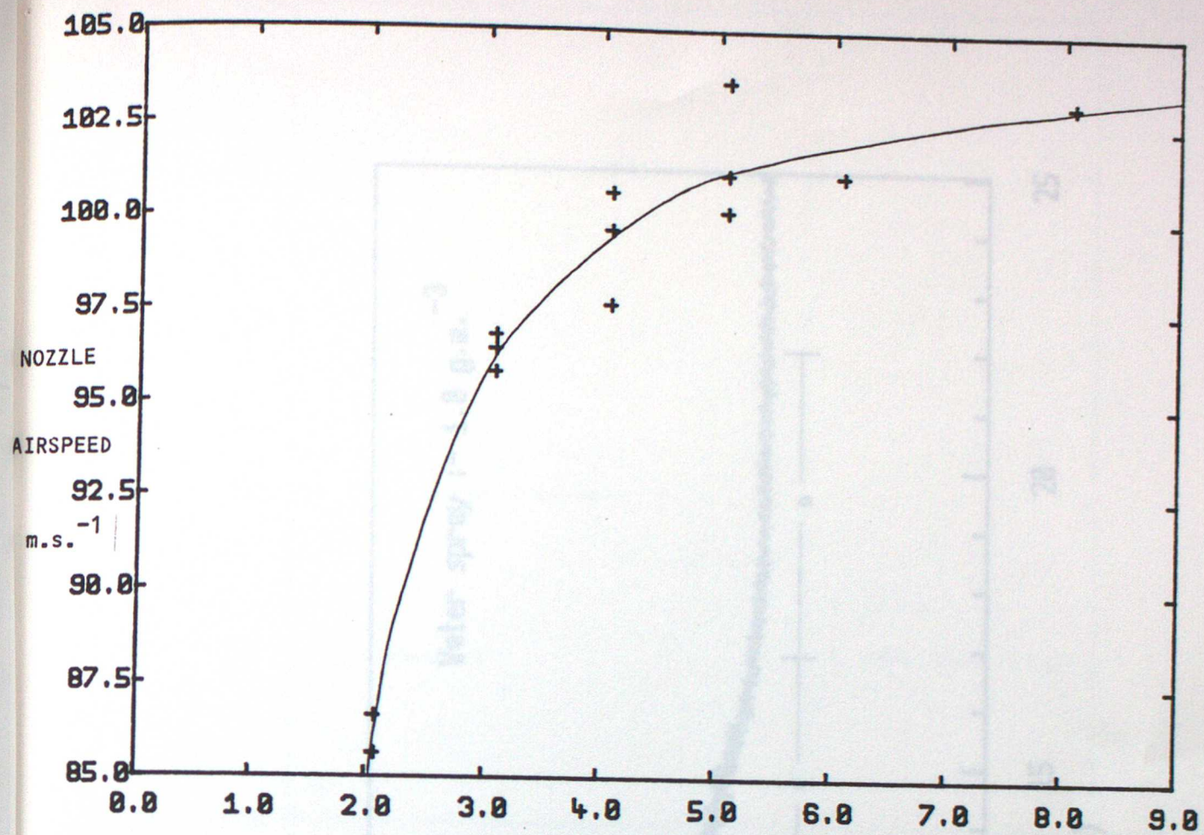

Fig.15a

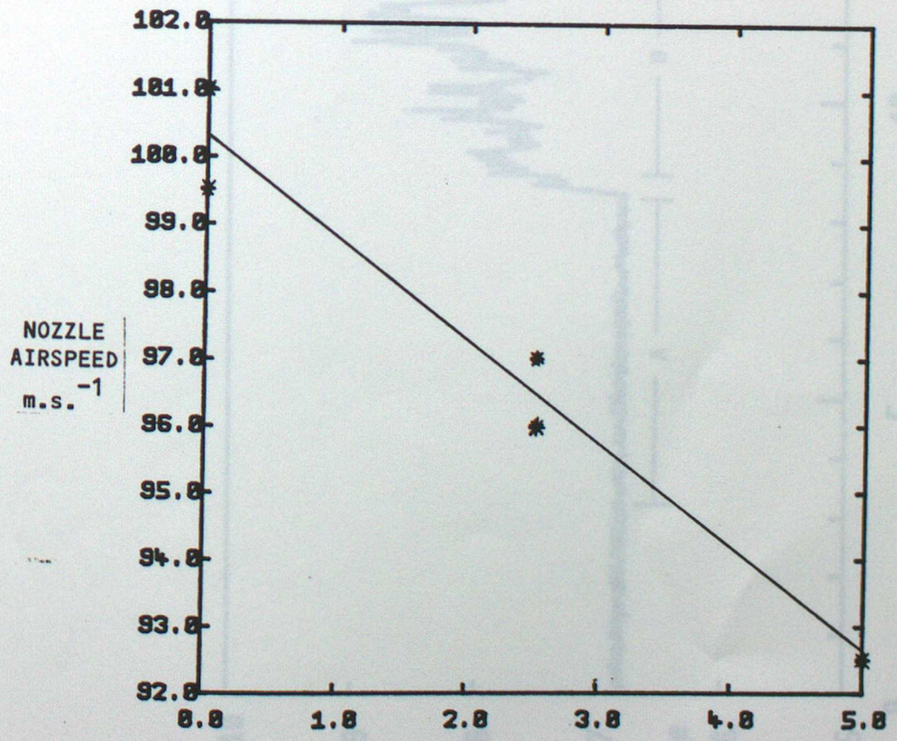

Fig.15b

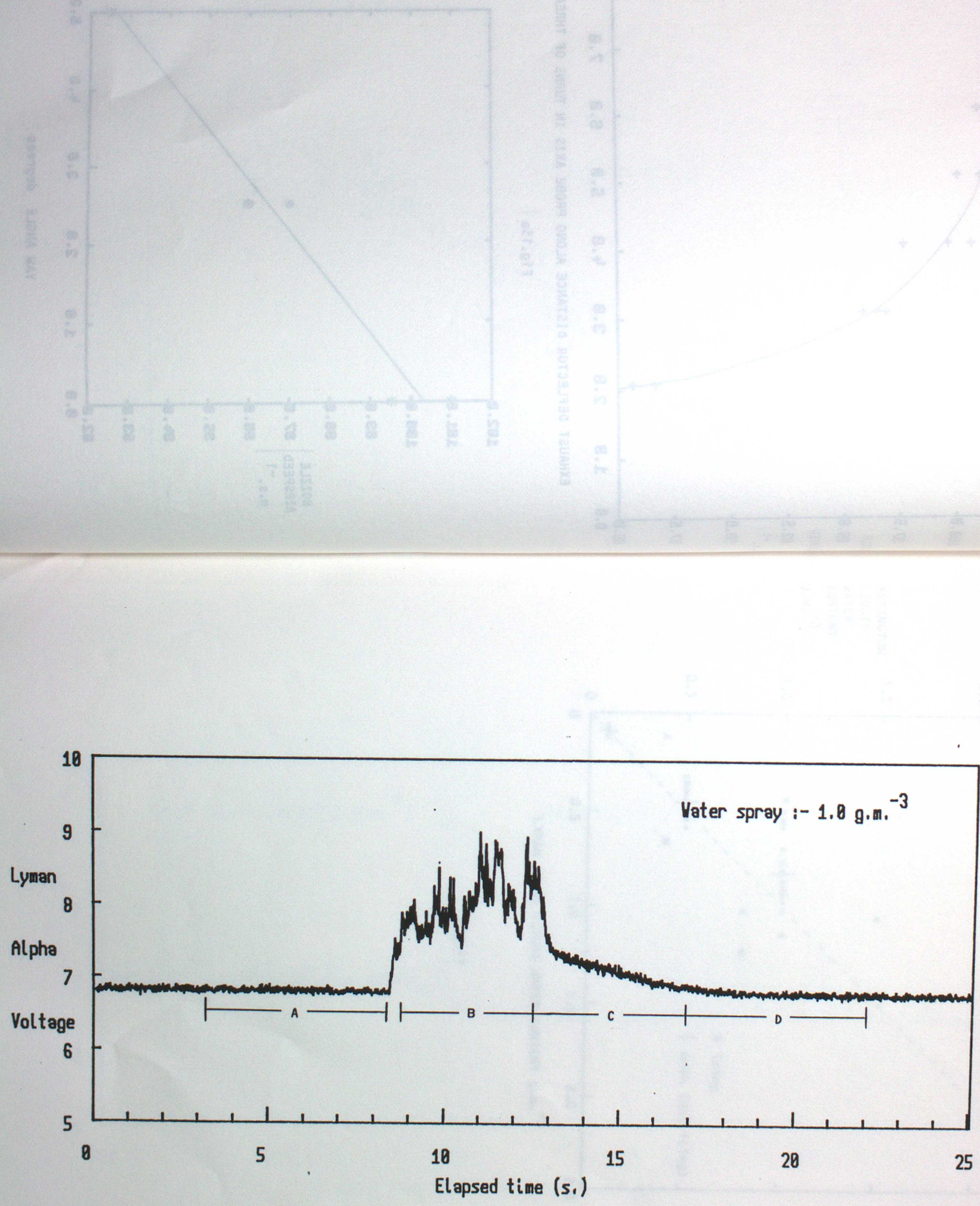
Water spray :- 1.0 g.m.$^{-3}$
Lyman Alpha Voltage
Elapsed time (s.)
A
B
C
D
10
9
8
7
6
5
0
5
10
15
20
25

Fig.16

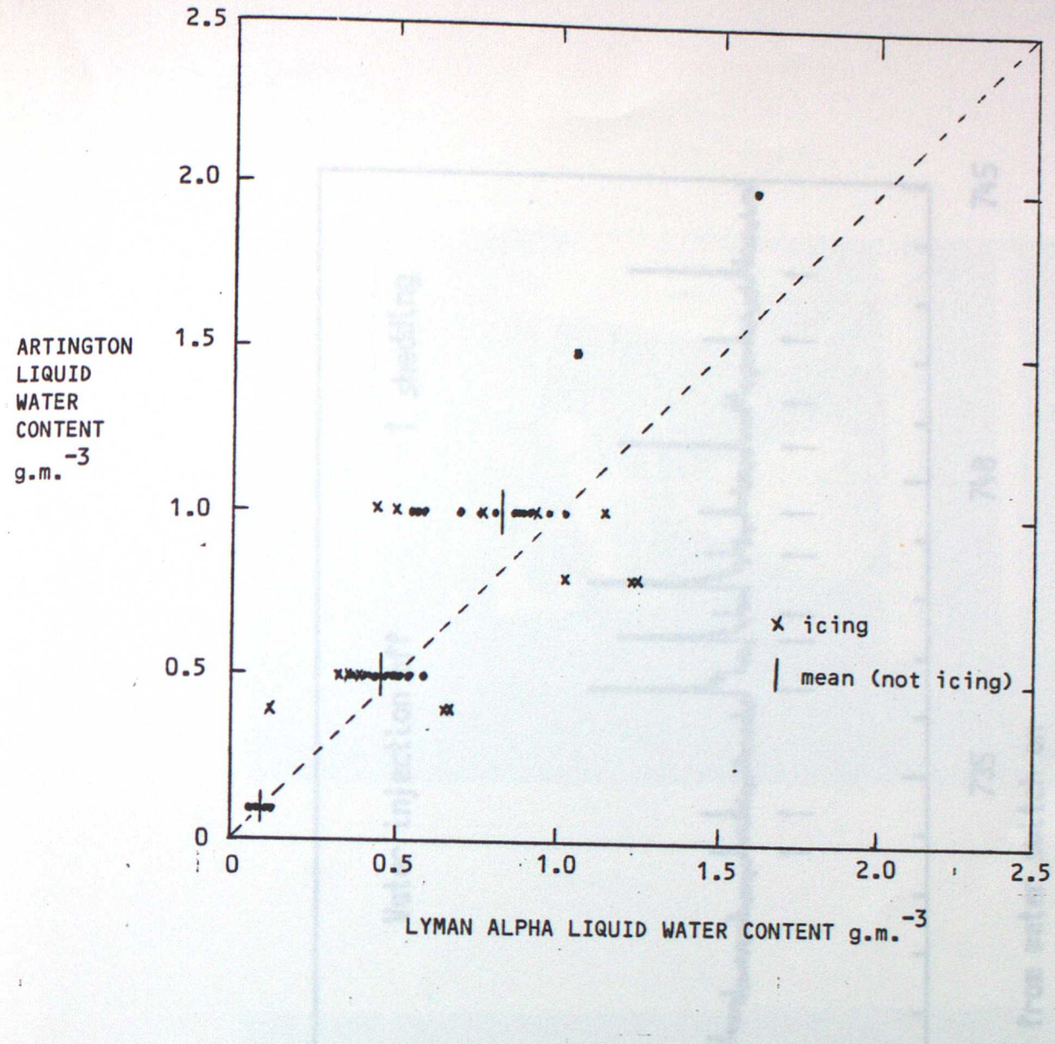
ARTINGTON LIQUID WATER CONTENT g.m.-3
LYMAN ALPHA LIQUID WATER CONTENT g.m.-3
0
0.5
1.0
1.5
2.0
2.5
x icing
| mean (not icing)

Fig.17

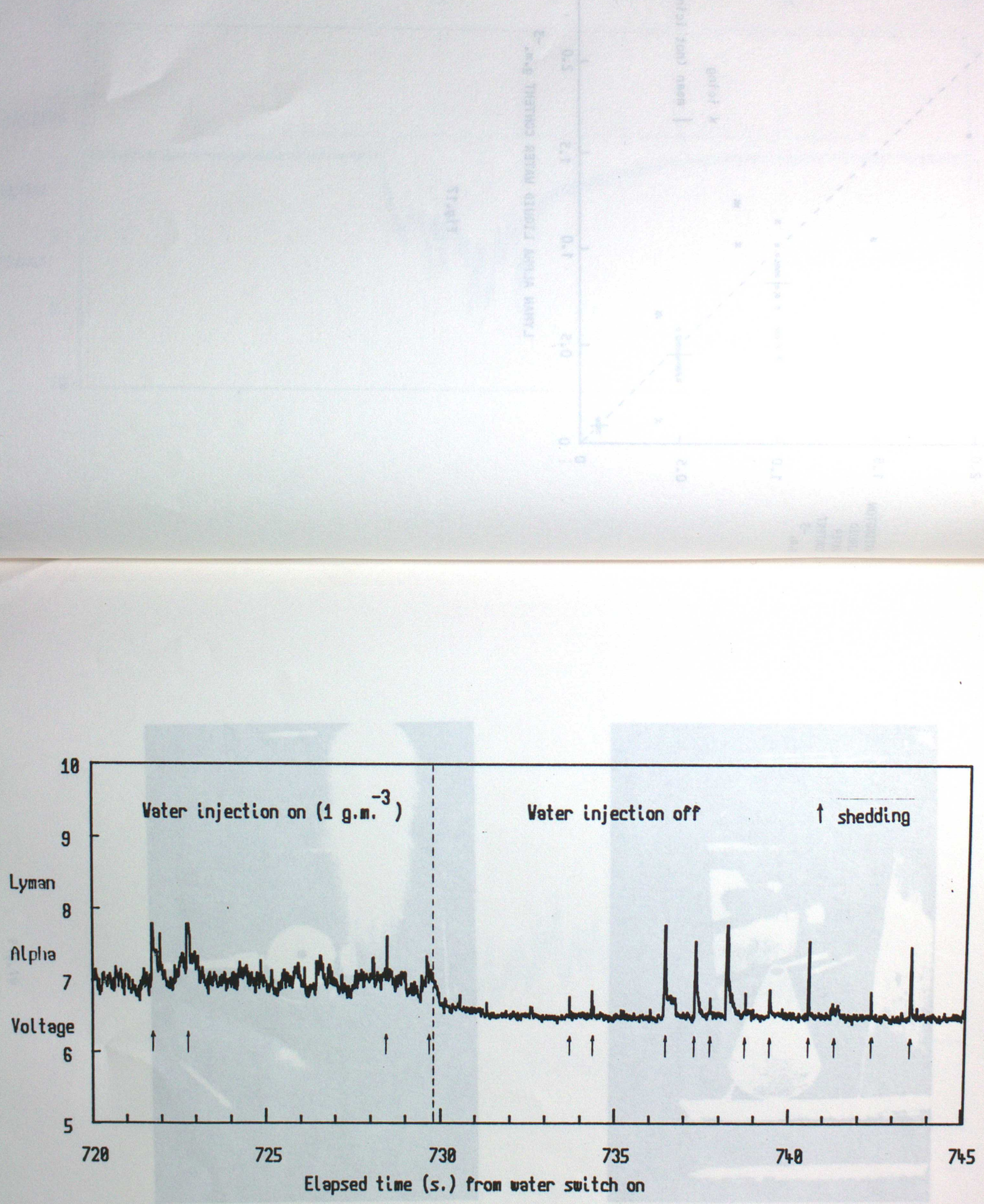
Water injection on (1 g.m.$^{-3}$)
Water injection off
shedding
Lyman Alpha Voltage
10
9
8
7
6
5
720
725
730
735
740
745
Elapsed time (s.) from water switch on

Fig.18

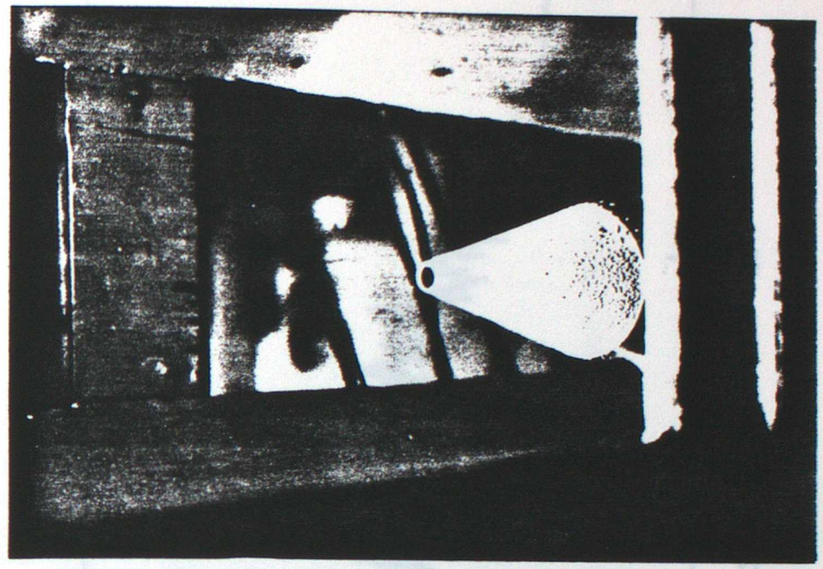

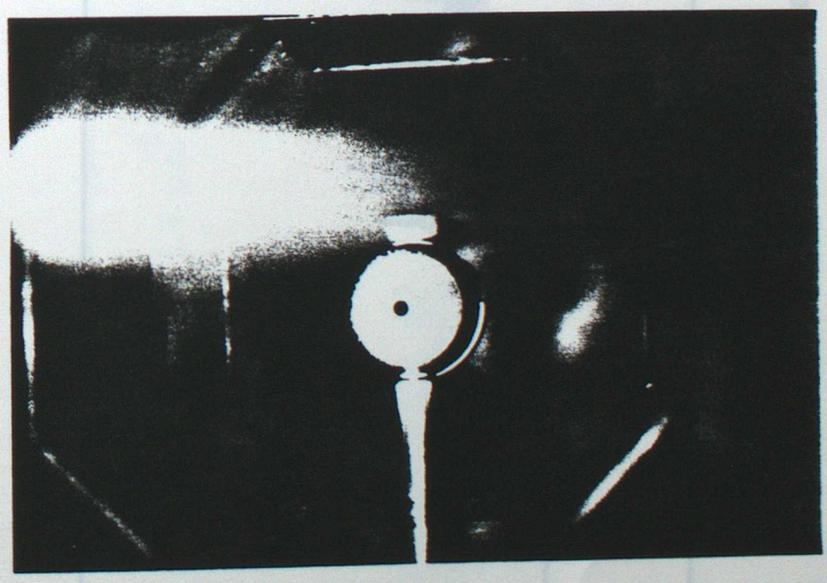

Fig.19

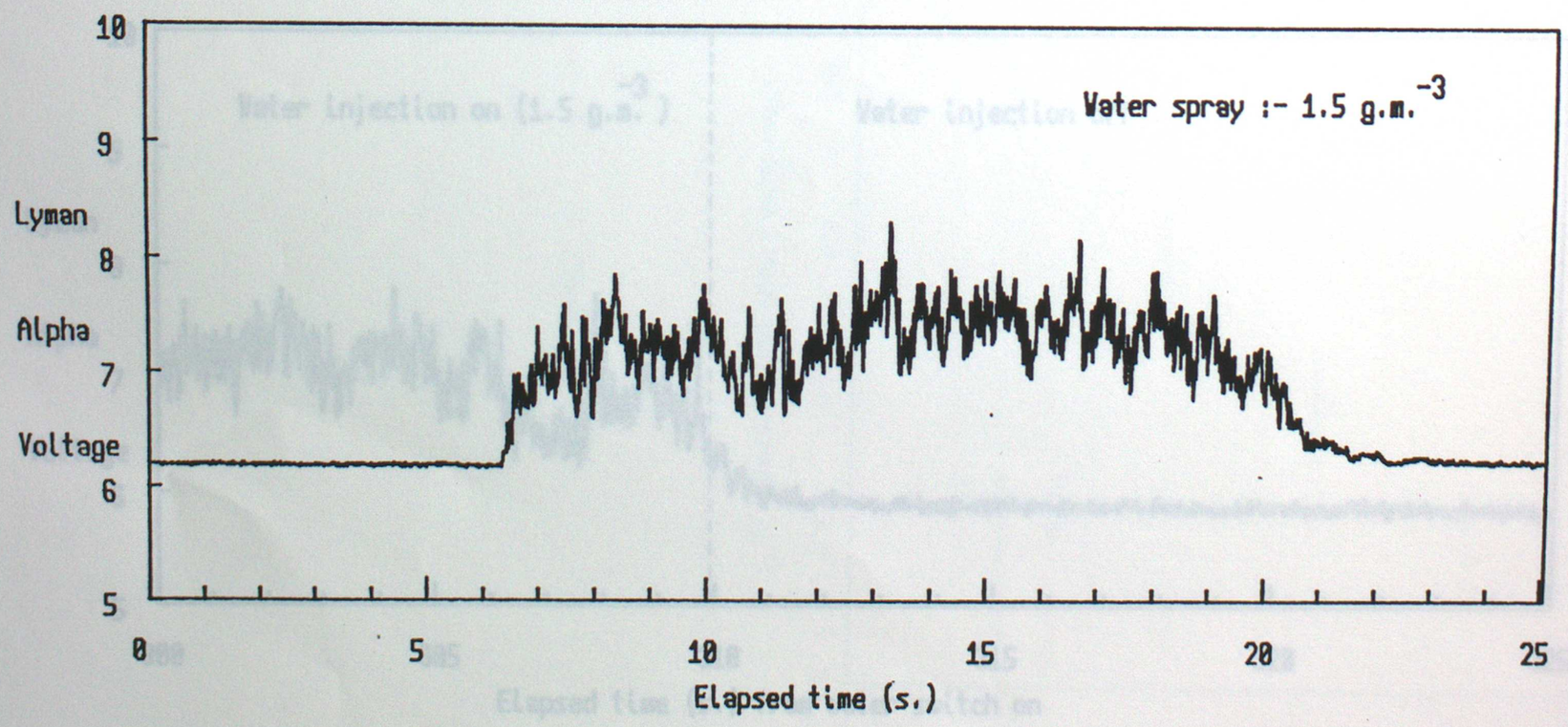
Water spray :- 1.5 g.m.-3
Lyman
Alpha
Voltage
10
9
8
7
6
5
0
5
10
15
20
25
Elapsed time (s.)

Fig.20

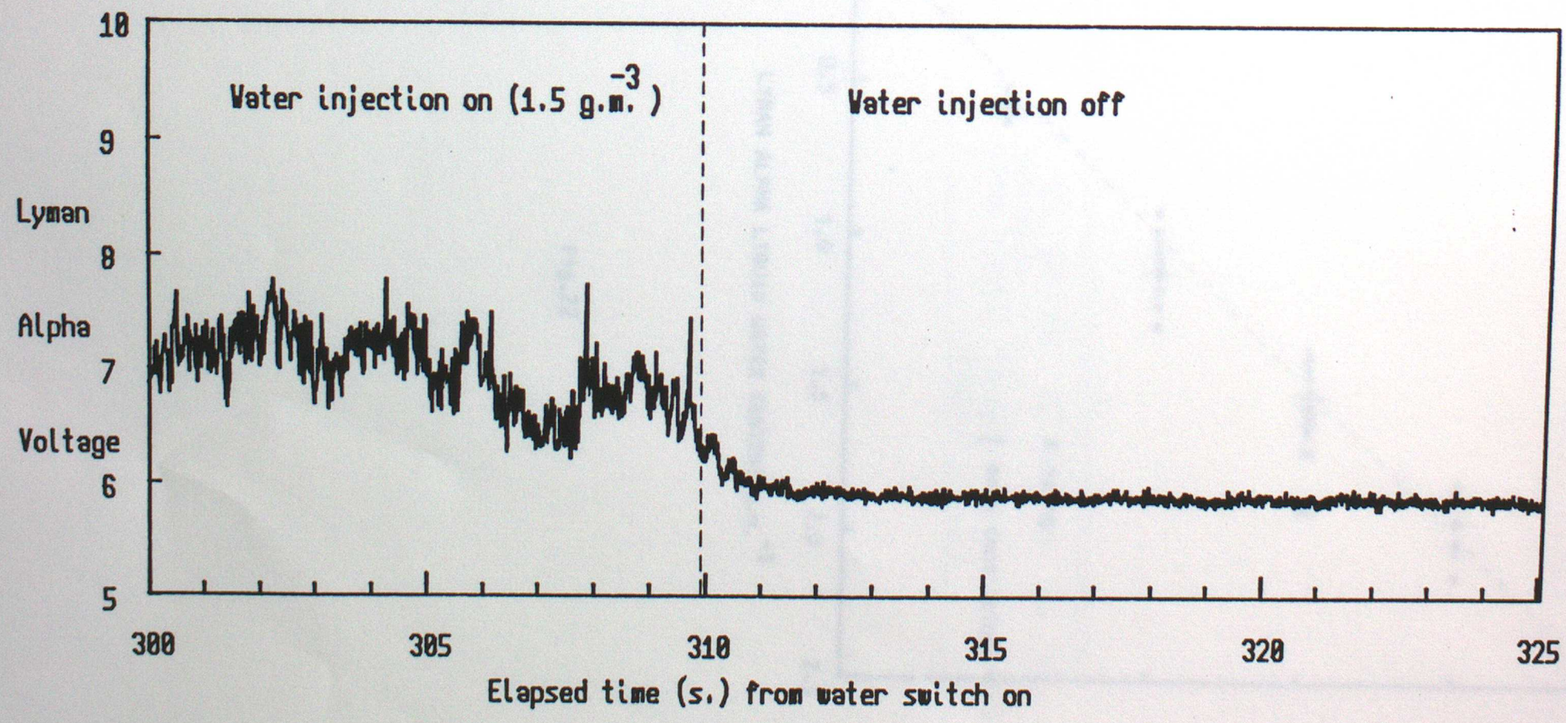
Water injection on (1.5 g.m.-3)
Water injection off
Lyman Alpha Voltage
10
9
8
7
6
5
300
305
310
315
320
325
Elapsed time (s.) from water switch on

Fig.21

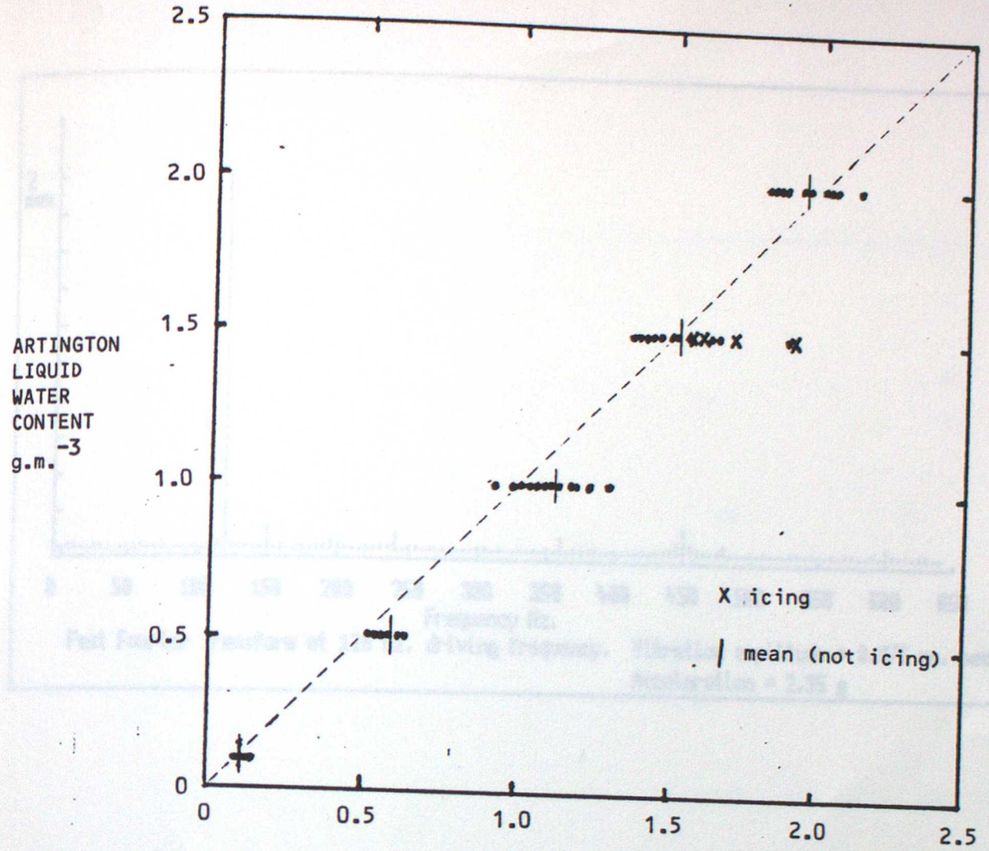
2.5
2.0
1.5
1.0
0.5
0
ARTINGTON
LIQUID
WATER
CONTENT
g.m.-3
X icing
mean (not icing)
0
0.5
1.0
1.5
2.0
2.5
LYMAN ALPHA LIQUID WATER CONTENT g.m.-3

Fig.22

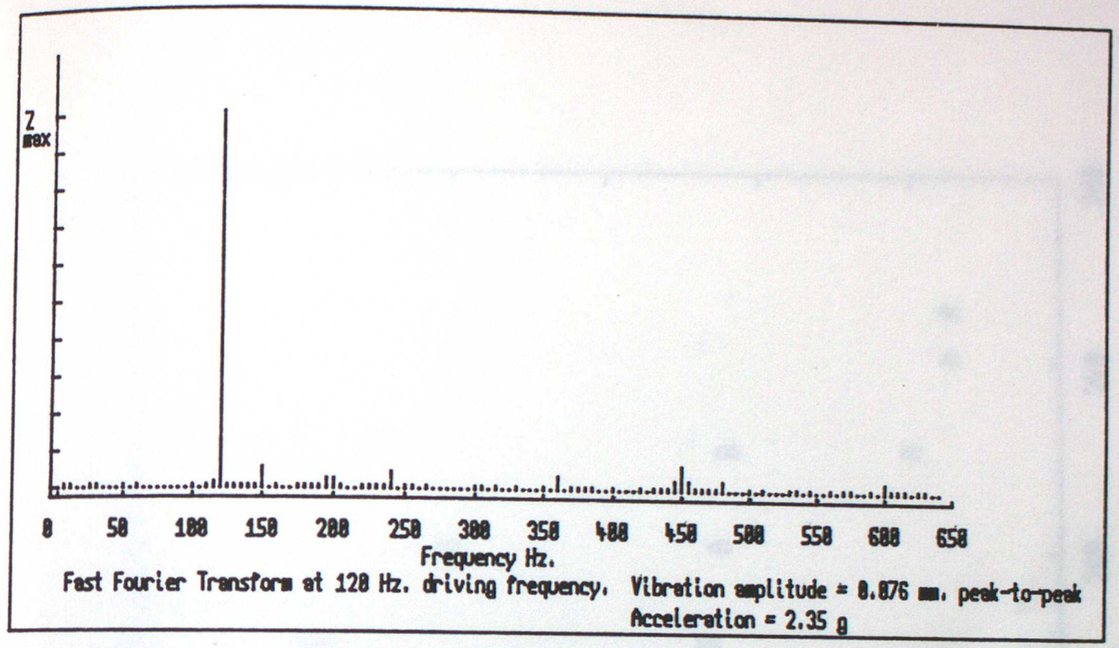

Fast Fourier Transform at 120 Hz. driving frequency. Vibration amplitude = 0.076 mm. peak-to-peak
Acceleration = 2.35 g

Fig.23

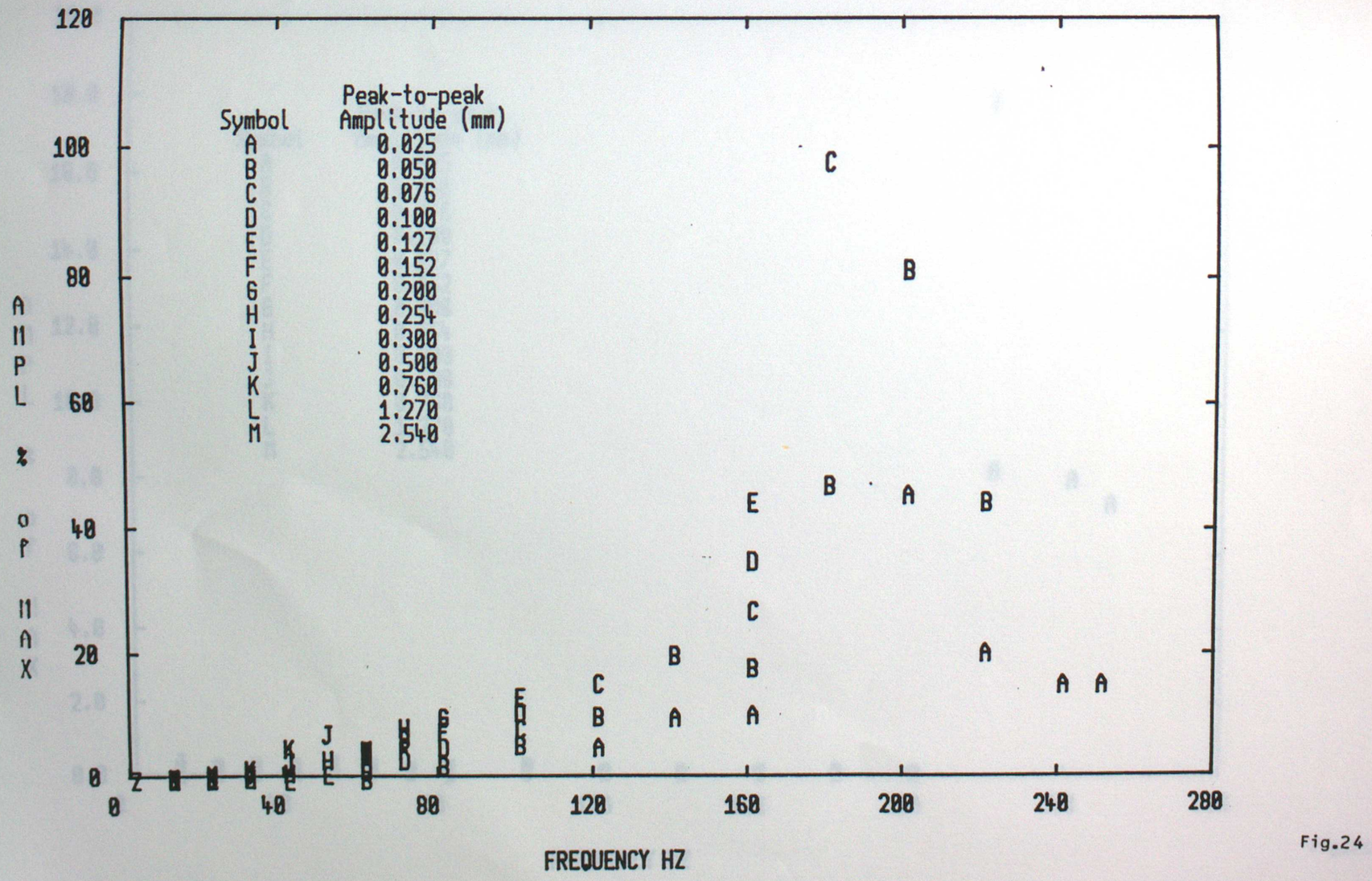
Peak-to-peak
Symbol Amplitude (mm)
A 0.025
B 0.050
C 0.076
D 0.100
E 0.127
F 0.152
G 0.200
H 0.254
I 0.300
J 0.500
K 0.760
L 1.270
M 2.540
AMPL % of MAX
FREQUENCY HZ
0
20
40
60
80
100
120
0
40
80
120
160
200
240
280

Fig.24

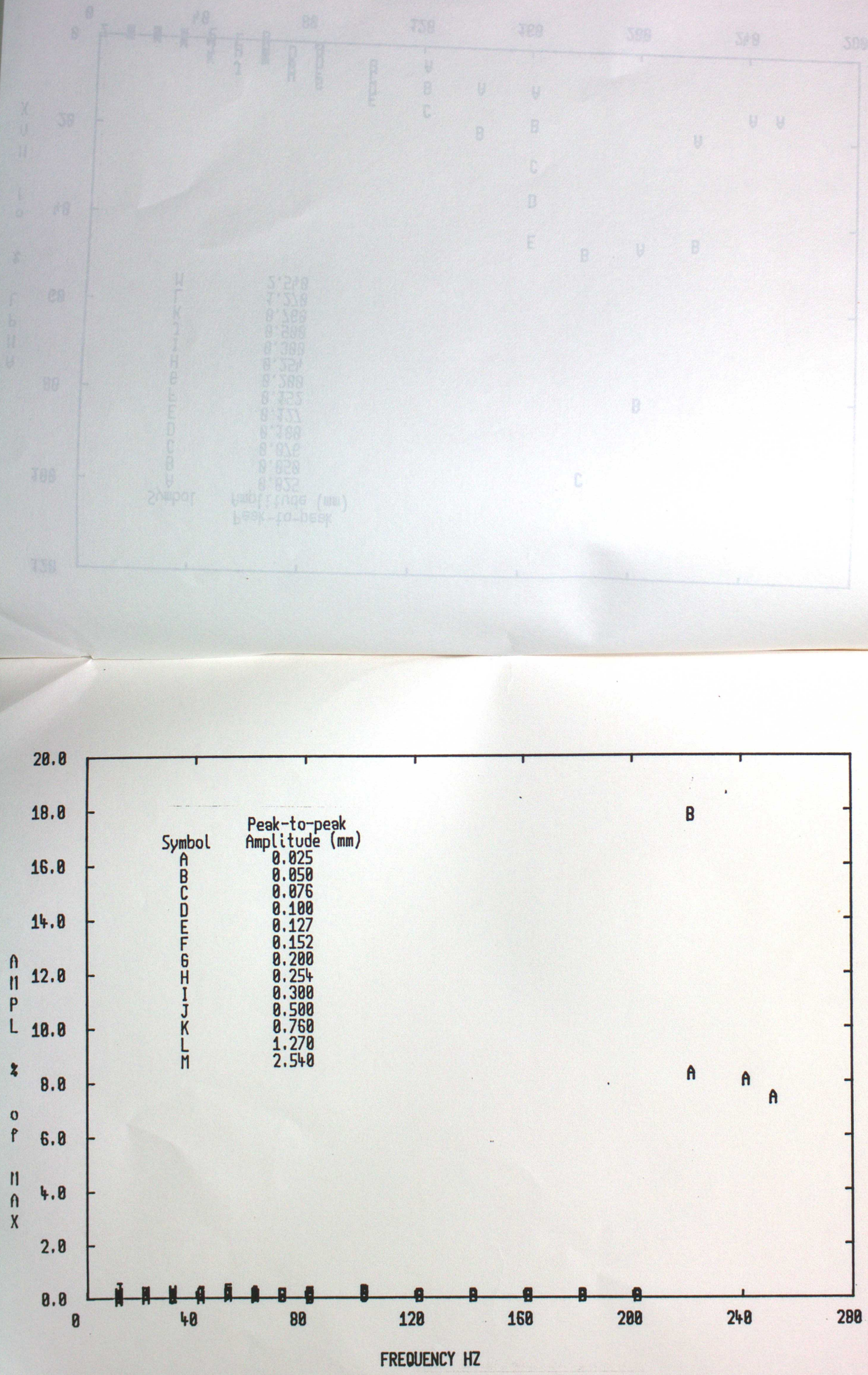
Peak-to-peak
Symbol Amplitude (mm)
A 0.025
B 0.050
C 0.076
D 0.100
E 0.127
F 0.152
G 0.200
H 0.254
I 0.300
J 0.500
K 0.760
L 1.270
M 2.540
AMPL % of MAX
20.0
18.0
16.0
14.0
12.0
10.0
8.0
6.0
4.0
2.0
0.0
0
40
80
120
160
200
240
280
FREQUENCY HZ

Fig.25